Optimal Quadratic Spline Collocation Methods for the Shallow Water Equations on the Sphere

Anita T. Layton[1]*, Christina C. Christara[2]†, and Kenneth R. Jackson[2]†

[1] *Department of Mathematics, University of North Carolina, Chapel Hill, North Carolina, USA.*
[2] *Department of Computer Science, University of Toronto, Toronto, Ontario, Canada.*

E-mail: [1]layton@amath.unc.edu, [2]{ccc, krj}@cs.toronto.edu

Abstract

In this study, we present numerical methods, based on the optimal quadratic spline collocation (OQSC) methods, for solving the shallow water equations (SWEs) in spherical coordinates. A quadratic spline collocation method approximates the solution of a differential problem by a quadratic spline. In the standard formulation, the quadratic spline is computed by making the residual of the differential equations zero at a set of collocation points; the resulting error is second order, while the error associated with quadratic spline interpolation is fourth order locally at certain points and third order globally. The OQSC methods generate approximations of the same order as quadratic spline interpolation. In the one-step OQSC method, the discrete differential operators are perturbed to eliminate low-order error terms, and a high-order approximation is computed using the perturbed operators. In the two-step OQSC method, a second-order approximation is generated first, using the standard formulation, and then a high-order approximation is computed in a second phase by perturbing the right sides of the equations appropriately.

In this implementation, the SWEs are discretized in time using the semi-Lagrangian semi-implicit scheme, which allows large timesteps while maintaining numerical stability, and in space using the OQSC methods. The resulting methods are efficient and yield stable and accurate representation of the meteorologically important Rossby waves. Moreover, by adopting

*Part of this work was done while the author was at the Department of Computer Science, University of Toronto.

†Partly supported by Natural Sciences and Engineering Research Council (NSERC) of Canada.

the Arakawa C-type grid, the methods also faithfully capture the group velocity of inertia-gravity waves.

Keywords: numerical weather prediction; finite element; semi-Lagrangian semi-implicit; Rossby stability; staggered grids.

Subject classifications: 65N35; 76B15; 86A10.

1 Introduction

In a companion paper [11], we present a finite element-based method, which discretizes the shallow water equations (SWEs) in time using the semi-Lagrangian semi-implicit (SLSI) method and in space using the quadratic spline Galerkin (QSG) method. In this paper, we present two alternative quadratic spline-based methods—the one-step and the two-step optimal quadratic collocation (OQSC) methods. These methods are described in Section 2. In Section 3, we present convergence results for the OQSC methods and compare their efficiencies with the QSG method and two low-order finite element methods. In Section 4, we analyze the performance of the methods on three staggered grids when applied to a simplified version of the SWEs; we conclude that, when discretized on the Arakawa C-type grid, these methods faithfully capture the group velocity of inertia-gravity waves, whereas neither the A- nor the B-grid produce comparably good results. This conclusion, which is consistent with the general agreement in the literature, is also supported by our numerical results for which we discretize Boyd's equatorial wave equations [1] using the A-, B-, and C-grids and set the initial conditions for the problem to generate gravitational modes.

The original form of the SWEs in spherical coordinates is presented in [8, 11]. Here we summarize the most important relations and notation; for a more detailed development see [11]. Since the longitudinal and latitudinal wind velocities u and v are multi-valued at the poles, the SWEs are rewritten in terms of the wind images, $U \equiv u\cos\theta/R$ and $V \equiv v\cos\theta/R$, as follows

$$\frac{dU}{dt} - fV + \frac{\phi_\lambda}{R^2} = 0, \tag{1}$$

$$\frac{dV}{dt} + fU + \frac{\cos\theta}{R^2}\phi_\theta + \delta = 0, \tag{2}$$

$$\cos\theta \frac{d}{dt}\log\phi + \left[\frac{U_\lambda}{\cos\theta} + V_\theta\right] = 0, \tag{3}$$

where d/dt denotes the Lagrangian derivative, R is the radius of the earth, Ω is its rotational speed, $f = 2\Omega\sin\theta$ is the Coriolis parameter, ϕ denotes the geopotential, and $\delta \equiv (U^2+V^2)\sin\theta/\cos^2\theta$. Along the longitude, functions are assumed periodic, whereas at the poles $(\theta = \pm\pi/2)$, homogeneous Dirichlet boundary conditions are imposed on the wind image components: $U(\lambda, \pm\pi/2) = V(\lambda, \pm\pi/2) = 0$. The latitudinal boundary conditions on ϕ are designed to mimic the behaviour of its spherical harmonic expansions [6], and are set to be homogeneous Neumann: $\phi_\theta(\lambda, \pm\pi/2) = 0$.

For an arbitrary function $\psi(\lambda,\theta,t)$, let $\tilde{\psi}^n$ denote the corresponding upstream function for the time interval t_n to t_{n+1}. That is, for the downstream gridpoint (λ,θ) associated with the displacement $(\delta\lambda^{n+1}, \delta\theta^{n+1})$, $\tilde{\psi}^n(\lambda,\theta) \equiv \psi(\lambda-\delta\lambda^{n+1}, \theta-\delta\theta^{n+1}, t_n)$. The Lagrangian derivative in the interval t_n to t_{n+1} is approximated by $d\tilde{\psi}^{n+\frac{1}{2}}/dt \approx (\psi^{n+1}-\tilde{\psi}^n)/\Delta t$. The gravity and Coriolis terms are treated semi-implicitly, that is, a function is averaged in time along particle trajectories: $\tilde{\psi}^{n+\frac{1}{2}} \approx (\psi^{n+1}+\tilde{\psi}^n)/2$.

When discretized in time using the two-level SLSI scheme, the motion equations (1) and (2) are rearranged to become

$$\begin{aligned}\begin{bmatrix} U^{n+1} \\ V^{n+1} \end{bmatrix} + \left(\frac{\Delta t}{2R^2}\right)\begin{bmatrix} c & d \\ -d & c \end{bmatrix}\begin{bmatrix} \phi_\lambda^{n+1} \\ \cos\tilde{\theta}\phi_\theta^{n+1} \end{bmatrix} \\ = \begin{bmatrix} a & b \\ -b & a \end{bmatrix}\begin{bmatrix} \tilde{U}^n \\ \tilde{V}^n \end{bmatrix} - \left(\frac{\Delta t}{2R^2}\right)\begin{bmatrix} c & d \\ -d & c \end{bmatrix}\begin{bmatrix} \tilde{\phi}_\lambda^n \\ \cos\tilde{\theta}\tilde{\phi}_\theta^n + 2R^2\tilde{\delta}^{n+\frac{1}{2}} \end{bmatrix} \equiv \begin{bmatrix} \tilde{R}_u^n \\ \tilde{R}_v^n \end{bmatrix},\end{aligned} \tag{4}$$

where a, b, c, and d are functions of θ defined by

$$a = \frac{1-\left(\frac{\Delta t\tilde{f}}{2}\right)^2}{1+\left(\frac{\Delta t\tilde{f}}{2}\right)^2}, \quad b = \frac{\Delta t\tilde{f}}{1+\left(\frac{\Delta t\tilde{f}}{2}\right)^2}, \quad c = \frac{1}{1+\left(\frac{\Delta t\tilde{f}}{2}\right)^2}, \quad d = \frac{\frac{\Delta t}{2}\tilde{f}}{1+\left(\frac{\Delta t\tilde{f}}{2}\right)^2}, \tag{5}$$

and where, for notational simplicity, $\tilde{f} \equiv \tilde{f}^{n+\frac{1}{2}}$ and $\tilde{\theta} \equiv \tilde{\theta}^{n+\frac{1}{2}}$.

The time-discretized continuity equation (3) is given by

$$\cos\tilde{\theta}^{n+\frac{1}{2}}\log\phi^{n+1} + \frac{\Delta t}{2}\left(\frac{U_\lambda^{n+1}}{\cos\tilde{\theta}^{n+\frac{1}{2}}} + V_\theta^{n+1}\right)$$

$$= \cos\tilde{\theta}^{n+\frac{1}{2}} \log\tilde{\phi}^n - \frac{\Delta t}{2}\left(\frac{\tilde{U}_\lambda^n}{\cos\tilde{\theta}^{n+\frac{1}{2}}} + \tilde{V}_\theta^n\right) \equiv \tilde{R}_\phi^n. \qquad (6)$$

2 The Optimal Quadratic Spline Collocation Methods

In this section, we explain how the two OQSC methods, originally derived for a single elliptic partial differential equation [2, 10] and later generalized to systems on unstaggered grids [12], can be modified to be applicable to the SWEs discretized on the staggered C-grid.

Let $\Delta\lambda = 2\pi/N_\lambda$ denote the meshsize in the λ-direction. Along the longitude, two uniform partitions that are staggered with respect to each other are defined:

$$\begin{aligned} \Delta_\lambda &\equiv \{0 = \lambda_0 < \lambda_1 < \cdots < \lambda_{N_\lambda} = 2\pi\} \text{ and} \\ \hat{\Delta}_\lambda &\equiv \left\{-\tfrac{\Delta\lambda}{2} = \hat{\lambda}_{-1} < \hat{\lambda}_0 < \cdots < \hat{\lambda}_{N_\lambda} = 2\pi + \tfrac{\Delta\lambda}{2}\right\}. \end{aligned}$$

The gridpoints in Δ_λ and $\hat{\Delta}_\lambda$ are chosen so that $\lambda_i = i\Delta\lambda$ for $i = 0, \ldots, N_\lambda$ and $\hat{\lambda}_i = (i + 1/2)\Delta\lambda$ for $i = -1, \ldots, N_\lambda$, respectively. Similarly, staggered partitions Δ_θ and $\hat{\Delta}_\theta$ are defined along the latitude by

$$\begin{aligned} \Delta_\theta &\equiv \left\{-\tfrac{\pi}{2} = \theta_0 < \theta_1 < \cdots < \theta_{N_\theta} = \tfrac{\pi}{2}\right\} \text{ and} \\ \hat{\Delta}_\theta &\equiv \left\{-\tfrac{\pi}{2} - \tfrac{\Delta\theta}{2} = \hat{\theta}_{-1} < \hat{\theta}_0 < \cdots < \hat{\theta}_{N_\theta} = \tfrac{\pi}{2} + \tfrac{\Delta\theta}{2}\right\}, \end{aligned}$$

where $\Delta\theta = \pi/N_\theta$, $\theta_j = -\pi/2 + j\Delta\theta$ for $j = 0, \ldots, N_\theta$ and $\hat{\theta}_j = -\pi/2 + (j+1/2)\Delta\theta$ for $j = -1, \ldots, N_\theta$. Let $\{\tau_{\lambda_i} = (\lambda_{i-1} + \lambda_i)/2\}_{i=1}^{N_\lambda}$ and $\{\hat{\tau}_{\lambda_i} = (\hat{\lambda}_{i-1} + \hat{\lambda}_i)/2\}_{i=0}^{N_\lambda}$ be the midpoints of Δ_λ and $\hat{\Delta}_\lambda$, respectively, and $\{\tau_{\theta_j} = (\theta_{j-1} + \theta_j)/2\}_{j=1}^{N_\theta}$ and $\{\hat{\tau}_{\theta_j} = (\hat{\theta}_{j-1} + \hat{\theta}_j)/2\}_{j=1}^{N_\theta - 1}$ be the midpoints of Δ_θ and $\hat{\Delta}_\theta$, respectively. For convenience, define $\tau_{\theta_0} \equiv \theta_0, \tau_{\theta_{N_\theta+1}} \equiv \theta_{N_\theta}, \hat{\tau}_{\theta_{-1}} \equiv -\pi/2, \hat{\tau}_{\theta_0} \equiv \hat{\theta}_0, \hat{\tau}_{\theta_{N_\theta}} \equiv \hat{\theta}_{N_\theta - 1}$, and $\hat{\tau}_{\theta_{N_\theta+1}} \equiv \pi/2$. Note also that the τ_{λ_i}'s and $\hat{\lambda}_i$'s almost coincide, as do the $\hat{\tau}_{\lambda_i}$'s and λ_i's, τ_{θ_j} and $\hat{\theta}_j$'s, and $\hat{\tau}_{\theta_j}$ and θ_j's, but for consistency with literature [2, 10] distinct notations are adopted.

A collocation method can be interpreted as a special case of the weighted residual method where the test functions are chosen to be delta functions associated with the collocation points, which, for quadratic splines, are usually chosen to be the midpoints of the partition. The standard quadratic spline collocation (QSC) method gives only second-order convergence, which is suboptimal, in the sense that the order of convergence of the spline collocation approximation is lower than that of the spline interpolant in the same approximation space. To obtain optimal solution approximations, the one-step or two-step correction method can be used [2, 10]. In the one-step method, the differential operators are perturbed to eliminate the low-order residual terms, and a fourth-order approximation is computed using the perturbed operators. In the two-step method, a second-order approximation is generated first using the standard formulation, and then a fourth-order approximation is computed in a second step by perturbing the right sides of the equations appropriately.

In order to derive the OQSC methods for the spatial discretization of the SWEs, we first recall selected results from [2, 10], and then extend them to the case that periodic conditions are assumed in one direction. We will present the results for an unstaggered partition, and later apply them to staggered partitions.

We adopt some convenient notation. Let $\mathcal{S}_\Delta$ be the quadratic spline space with respect to some partition Δ. Let D_s^k denote the k-th derivative operator with respect to the variable s. For an arbitrary function $\psi(\theta)$, let $\psi_j \equiv \psi(\tau_{\theta_j})$ for $j = 0, \ldots, N_\theta + 1$. Define the difference operator Λ_θ by $(\Lambda_\theta \psi)_j \equiv (\psi_{j-1} - 2\psi_j + \psi_{j+1})/\Delta\theta^2$, for $j = 2, \ldots, N_\theta - 1$. The following results are given in [10].

Theorem 1 *Let $\psi_I(\theta) \in \mathcal{S}_{\Delta_\theta}$ be the quadratic spline interpolant of a function $\psi(\theta) \in C^6$ such that*

$$(\psi_I)_j = \psi_j, \tag{7}$$

for $j = 1, \ldots, N_\theta$, and

$$(\psi_I)_j = \psi_j - \frac{\Delta\theta^4}{128}(D_\theta^4 \psi)_j, \tag{8}$$

for $j = 0$ and $j = N_\theta + 1$. Then the following relations hold:

$$(D_\theta \psi_I)_j = (D_\theta \psi)_j + \frac{\Delta\theta^2}{24}(D_\theta^3 \psi)_j + \mathcal{O}(\Delta\theta^4), \quad j = 1, \ldots, N_\theta, \tag{9}$$

$$(D_\theta \psi_I)(\theta_j) = (D_\theta \psi)(\theta_j) - \frac{\Delta\theta^2}{12}(D_\theta^3 \psi)(\theta_j) + \mathcal{O}(\Delta\theta^4), \quad j = 0, \ldots, N_\theta, \tag{10}$$

$$(D_\theta^3 \psi)_j = \Lambda_\theta (D_\theta \psi_I)_j + \mathcal{O}(\Delta\theta^2), \quad j = 2, \ldots, N_\theta - 1, \tag{11}$$

$$(D_\theta^3 \psi)_0 = \frac{1}{2}\left(5\Lambda_\theta (D_\theta \psi_I)_2 - 3\Lambda_\theta (D_\theta \psi_I)_3\right) + \mathcal{O}(\Delta\theta^2), \tag{12}$$

$$(D_\theta^3\psi)_1 = 2\Lambda_\theta(D_\theta\psi_I)_2 - \Lambda_\theta(D_\theta\psi_I)_3 + \mathcal{O}(\Delta\theta^2), \tag{13}$$

$$(D_\theta^3\psi)_{N_\theta} = 2\Lambda_\theta(D_\theta\psi_I)_{N_\theta-1} - \Lambda_\theta(D_\theta\psi_I)_{N_\theta-2} + \mathcal{O}(\Delta\theta^2), \tag{14}$$

$$(D_\theta^3\psi)_{N_\theta+1} = \frac{1}{2}\left(5\Lambda_\theta(D_\theta\psi_I)_{N_\theta-1} - 3\Lambda_\theta(D_\theta\psi_I)_{N_\theta-2}\right) + \mathcal{O}(\Delta\theta^2). \tag{15}$$

For brevity, define another difference operator Λ'_θ by

$$\begin{aligned}
(\Lambda'_\theta\psi)_0 &\equiv \frac{1}{2}\left(5\Lambda_\theta(D_\theta\psi)_2 - 3\Lambda_\theta(D_\theta\psi)_3\right) = \frac{5\psi_1 - 13\psi_2 + 11\psi_3 - 3\psi_4}{2\Delta\theta^2},\\
(\Lambda'_\theta\psi)_1 &\equiv 2\Lambda_\theta(D_\theta\psi)_2 - \Lambda_\theta(D_\theta\psi)_3 \qquad = \frac{2\psi_1 - 5\psi_2 + 4\psi_3 - \psi_4}{\Delta\theta^2},\\
(\Lambda'_\theta\psi)_j &\equiv (\Lambda_\theta\psi)_j, \quad j = 2, \ldots, N_\theta - 1,\\
(\Lambda'_\theta\psi)_{N_\theta} &\equiv 2\Lambda_\theta(D_\theta\psi)_{N_\theta-1} - \Lambda_\theta(D_\theta\psi)_{N_\theta-2} = \frac{2\psi_{N_\theta} - 5\psi_{N_\theta-1} + 4\psi_{N_\theta-2} - \psi_{N_\theta-3}}{\Delta\theta^2},\\
(\Lambda'_\theta\psi)_{N_\theta+1} &\equiv \frac{1}{2}\left(5\Lambda_\theta(D_\theta\psi)_{N_\theta-1} - 3\Lambda_\theta(D_\theta\psi)_{N_\theta-2}\right)\\
&= \frac{5\psi_{N_\theta} - 13\psi_{N_\theta-1} + 11\psi_{N_\theta-2} - 3\psi_{N_\theta-3}}{2\Delta\theta^2}.
\end{aligned}$$

Then, relations (11)–(15) become

$$(D_\theta^3\psi)_j = \Lambda'_\theta(D_\theta\psi_I)_j + \mathcal{O}(\Delta\theta^2), \quad j = 0, \ldots, N_\theta + 1. \tag{16}$$

We extend the above results to periodic quadratic splines. A quadratic spline ψ is periodic in $[\lambda_0, \lambda_{N_\lambda}]$ ($= [0, 2\pi]$), when $\psi(\lambda_0) = \psi(\lambda_{N_\lambda})$ and $D_\lambda\psi(\lambda_0) = D_\lambda\psi(\lambda_{N_\lambda})$. Since periodicity in $[0, 2\pi]$ along the λ direction is assumed for all functions throughout this paper, we will omit the interval of periodicity for brevity. For an arbitrary function $\psi(\lambda)$, let $\psi_i \equiv \psi(\tau_{\lambda_i})$ for $i = 1, \ldots, N_\lambda$. Define the difference operator Λ'_λ by $(\Lambda'_\lambda\psi)_i \equiv (\psi_{i-1} - 2\psi_i + \psi_{i+1})/\Delta\lambda^2$ for $i = 2, \ldots, N_\lambda - 1$, $(\Lambda'_\lambda\psi)_1 \equiv (\psi_{N_\lambda} - 2\psi_1 + \psi_2)/\Delta\lambda^2$ and $(\Lambda'_\lambda\psi)_{N_\lambda} \equiv (\psi_{N_\lambda-1} - 2\psi_{N_\lambda} + \psi_1)/\Delta\lambda^2$. The proof of the following theorem is similar to the proof of Theorem 1 (see [10]) and is omitted for brevity.

Theorem 2 *Let $\psi_I(\lambda) \in \mathcal{S}_{\Delta_\lambda}$ be the periodic quadratic spline interpolant of a periodic function $\psi(\lambda) \in C^6$ such that*

$$(\psi_I)_i = \psi_i, \tag{17}$$

for $i = 1, \ldots, N_\lambda$. Then the following relations hold:

$$(D_\lambda\psi_I)_i = (D_\lambda\psi)_i + \frac{\Delta\lambda^2}{24}(D_\lambda^3\psi)_i + \mathcal{O}(\Delta\lambda^4), \quad i = 1, \ldots, N_\lambda, \tag{18}$$

$$(D_\lambda \psi_I)(\lambda_i) = (D_\lambda \psi)(\lambda_i) - \frac{\Delta\lambda^2}{12}(D_\lambda^3 \psi)(\lambda_i) + \mathcal{O}(\Delta\lambda^4), \quad i = 1, \ldots, N_\lambda, \tag{19}$$

$$(D_\lambda^3 \psi)_i = \Lambda'_\lambda (D_\lambda \psi_I)_i + \mathcal{O}(\Delta\lambda^2), \quad i = 1, \ldots, N_\lambda. \tag{20}$$

In [2], the results of Theorem 1 are extended to two dimensions using a tensor product approach. Following a similar approach, we do the same, assuming all functions are periodic in the λ direction. Consider the biquadratic spline space $\mathcal{S}_{\Delta_\lambda \times \Delta_\theta}$ associated with the partition $\Delta_\lambda \times \Delta_\theta$. A biquadratic spline $\psi(\lambda, \theta) \in \mathcal{S}_{\Delta_\lambda \times \Delta_\theta}$ is periodic in λ, when $\psi(\lambda_0, \theta) = \psi(\lambda_{N_\lambda}, \theta)$ and $D_\lambda \psi(\lambda_0, \theta) = D_\lambda \psi(\lambda_{N_\lambda}, \theta)$ $\forall \theta$ in the θ-domain, which, for Δ_θ, is $[-\pi/2, +\pi/2]$. For an arbitrary function $\psi(\lambda, \theta)$, let $\psi_{i,j} \equiv \psi(\tau_{\lambda_i}, \tau_{\theta_j})$. We extend the definitions of Λ'_θ and Λ'_λ to functions of two variables in the obvious way. That is,

$$\begin{aligned}
(\Lambda'_\theta \psi)_{i,0} &\equiv \frac{5\psi_{i,1} - 13\psi_{i,2} + 11\psi_{i,3} - 3\psi_{i,4}}{2\Delta\theta^2}, \\
(\Lambda'_\theta \psi)_{i,1} &\equiv \frac{2\psi_{i,1} - 5\psi_{i,2} + 4\psi_{i,3} - \psi_{i,4}}{\Delta\theta^2}, \\
(\Lambda'_\theta \psi)_{i,j} &\equiv \frac{\psi_{i,j-1} - 2\psi_{i,j} + \psi_{i,j+1}}{\Delta\theta^2}, \qquad j = 2, \ldots, N_\theta - 1, \\
(\Lambda'_\theta \psi)_{i,N_\theta} &\equiv \frac{2\psi_{i,N_\theta} - 5\psi_{i,N_\theta-1} + 4\psi_{i,N_\theta-2} - \psi_{i,N_\theta-3}}{\Delta\theta^2}, \\
(\Lambda'_\theta \psi)_{i,N_\theta+1} &\equiv \frac{5\psi_{i,N_\theta} - 13\psi_{i,N_\theta-1} + 11\psi_{i,N_\theta-2} - 3\psi_{i,N_\theta-3}}{2\Delta\theta^2},
\end{aligned}$$

for $i = 1, \ldots, N_\lambda$, and

$$\begin{aligned}
(\Lambda'_\lambda \psi)_{1,j} &\equiv \frac{\psi_{N_\lambda,j} - 2\psi_{1,j} + \psi_{2,j}}{\Delta\lambda^2}, \\
(\Lambda'_\lambda \psi)_{i,j} &\equiv \frac{\psi_{i-1,j} - 2\psi_{i,j} + \psi_{i+1,j}}{\Delta\lambda^2}, \qquad i = 2, \ldots, N_\lambda - 1, \\
(\Lambda'_\lambda \psi)_{N_\lambda,j} &\equiv \frac{\psi_{N_\lambda-1,j} - 2\psi_{N_\lambda,j} + \psi_{1,j}}{\Delta\lambda^2},
\end{aligned} \tag{21}$$

for $j = 0, \ldots, N_\theta + 1$. Using techniques similar to those in [2], we are now ready to present the following theorem.

Theorem 3 *Let $\psi_I(\lambda, \theta) \in \mathcal{S}_{\Delta_\lambda \times \Delta_\theta}$ be the periodic in λ biquadratic spline interpolant of a periodic in λ function $\psi(\lambda, \theta) \in C^6$, defined by*

$$(\psi_I)_{i,j} = \psi_{i,j}, \tag{22}$$

for $i = 1, \ldots, N_\lambda$ and $j = 1, \ldots, N_\theta$, and

$$(\psi_I)_{i,j} = \psi_{i,j} - \frac{\Delta\theta^4}{128}(D_\theta^4\psi)_{i,j}, \tag{23}$$

for $i = 1, \ldots, N_\lambda$, and $j = 0, N_\theta + 1$. Then, for $i = 1, \ldots, N_\lambda$, the following relations hold:

$$(D_\theta\psi_I)_{i,j} = (D_\theta\psi)_{i,j} + \frac{\Delta\theta^2}{24}(D_\theta^3\psi)_{i,j} + \mathcal{O}(\Delta\theta^4), \quad j = 1, \ldots, N_\theta, \tag{24}$$

$$(D_\theta\psi_I)(\tau_{\lambda_i}, \theta_j) = (D_\theta\psi)(\tau_{\lambda_i}, \theta_j) - \frac{\Delta\theta^2}{12}(D_\theta^3\psi)(\tau_{\lambda_i}, \theta_j) + \mathcal{O}(\Delta\theta^4), \quad j = 0, \ldots, N_\theta, \tag{25}$$

$$(D_\theta^3\psi)_{i,j} = \Lambda'_\theta(D_\theta\psi_I)_{i,j} + \mathcal{O}(\Delta\theta^2), \quad j = 0, \ldots, N_\theta + 1, \tag{26}$$

$$(D_\lambda\psi_I)_{i,j} = (D_\lambda\psi)_{i,j} + \frac{\Delta\lambda^2}{24}(D_\lambda^3\psi)_{i,j} + \mathcal{O}(\Delta\lambda^4), \quad j = 1, \ldots, N_\theta, \tag{27}$$

$$(D_\lambda\psi_I)(\lambda_i, \tau_{\theta_j}) = (D_\lambda\psi)(\lambda_i, \tau_{\theta_j}) - \frac{\Delta\lambda^2}{12}(D_\lambda^3\psi)(\lambda_i, \tau_{\theta_j}) + \mathcal{O}(\Delta\lambda^4), \quad j = 1, \ldots, N_\theta, \tag{28}$$

$$(D_\lambda^3\psi)_{i,j} = \Lambda'_\lambda(D_\lambda\psi_I)_{i,j} + \mathcal{O}(\Delta\lambda^2), \quad j = 0, \ldots, N_\theta + 1. \tag{29}$$

2.1 Derivation of OQSC Methods on Staggered Grids

In this subsection, we extend the OQSC methods to staggered grids and apply the resulting methods to the coupled SWEs discretized spatially on the C-grid. When discretized on a C-grid [8], the target functions U, V, and ϕ in (4) and (6) are approximated in the biquadratic spline spaces $\mathcal{S}_{\Delta_1}$, $\mathcal{S}_{\Delta_2}$ and $\mathcal{S}_{\Delta_3}$, defined on the induced grid partitions $\Delta_1 \equiv \hat{\Delta}_\lambda \times \Delta_\theta$, $\Delta_2 \equiv \Delta_\lambda \times \hat{\Delta}_\theta$, and $\Delta_3 \equiv \Delta_\lambda \times \Delta_\theta$, respectively. Each target function is approximated by a linear combination of biquadratic spline basis functions. Whenever possible, the adjusted basis functions given in [11], which satisfy the boundary conditions, are used.

More specifically, U and V are approximated by linear combinations of $\{\hat{\beta}_i^P(\lambda)\beta_j^D(\theta)\}_{i=1,j=1}^{N_\lambda,N_\theta}$, and $\{\beta_i^P(\lambda)\hat{\beta}_j^D(\theta)\}_{i=1,j=0}^{N_\lambda,N_\theta}$, respectively, as in [11]. In this way, the approximations satisfy the appropriate boundary conditions by construction. The approximation to ϕ in the first step of the two-step OQSC method is a linear combination of $\{\beta_i^P(\lambda)\beta_j^N(\theta)\}_{i=1,j=1}^{N_\lambda,N_\theta}$. Thus it satisfies periodic conditions in the $\lambda-$direction and homogeneous Neumann conditions in the $\theta-$direction by construction. In the second step of the two-step OQSC and in the one-step OQSC method the approximations to ϕ are a linear combination of $\{\beta_i^P(\lambda)\beta_j(\theta)\}_{i=1,j=0}^{N_\lambda,N_\theta+1}$, and the boundary conditions are imposed explicitly. This is because the approximations to ϕ in these cases satisfy non-homogeneous Neumann conditions in the $\theta-$direction, due to a perturbation on the boundary as described in Sections 2.2 and 2.3. When computing the degrees of freedom (spline coefficients) of the approximations to ϕ in the second step of the two-step OQSC and in the one-step OQSC method, we first compute the degrees of freedom corresponding to the "interior" basis functions $\{\beta_i^P(\lambda)\beta_j(\theta)\}_{i=1,j=1}^{N_\lambda,N_\theta}$, by eliminating the rest of the degrees of freedom, then recover the degrees of freedom corresponding to the "boundary" basis functions $\{\beta_i^P(\lambda)\beta_0(\theta), \beta_i^P(\lambda)\beta_{N_\theta+1}(\theta)\}_{i=1}^{N_\lambda}$, from the equations corresponding to the boundary conditions.

The collocation points for Δ_1, Δ_2 and Δ_3 are chosen to be $\{(\hat{\tau}_{\lambda_i}, \tau_{\theta_j})\}_{i=1,j=1}^{N_\lambda,N_\theta}$, $\{(\tau_{\lambda_i}, \hat{\tau}_{\theta_j})\}_{i=1,j=0}^{N_\lambda,N_\theta}$ and $\{(\tau_{\lambda_i}, \tau_{\theta_j})\}_{i=1,j=1}^{N_\lambda,N_\theta}$, respectively. Note that the collocation points $\hat{\tau}_{\theta_0} = \hat{\theta}_0$ and $\hat{\tau}_{\theta_{N_\theta}} = \hat{\theta}_{N_\theta-1}$ are gridpoints of $\hat{\Delta}_\theta$.

Consider the solution U^{n+1} of the time-discretized SWEs (4) and (6), and let $U_I^{n+1} \in \mathcal{S}_{\Delta_1}$ be its biquadratic spline interpolant, such that

$$U_I^{n+1}(\hat{\tau}_{\lambda_i}, \tau_{\theta_j}) = U^{n+1}(\hat{\tau}_{\lambda_i}, \tau_{\theta_j}) \tag{30}$$

for $i = 1, \ldots, N_\lambda$ and $j = 1, \ldots, N_\theta$, and

$$U_I^{n+1}(\hat{\tau}_{\lambda_i}, \tau_{\theta_j}) = U^{n+1}(\hat{\tau}_{\lambda_i}, \tau_{\theta_j}) - \frac{\Delta\theta^4}{128} D_\theta^4 U^{n+1}(\hat{\tau}_{\lambda_i}, \tau_{\theta_j}), \tag{31}$$

for $i = 1, \ldots, N_\lambda$, and $j = 0, N_\theta + 1$. The above interpolant is constructed to facilitate the mathematical derivation of the OQSC methods, but it is not used in the computation. Similarly, let $V_I^{n+1} \in \mathcal{S}_{\Delta_2}$ be the biquadratic spline interpolant of V^{n+1}, and $\phi_I^{n+1} \in \mathcal{S}_{\Delta_3}$ and $\zeta_I^{n+1} \in \mathcal{S}_{\Delta_3}$ be the interpolants of ϕ^{n+1} and $\log \phi^{n+1}$, respectively.

By substituting the spline interpolants U_I^{n+1}, V_I^{n+1}, ϕ_I^{n+1} and ζ_I^{n+1} into the time-discretized equations (4) (two equations) and (6), evaluating at $\{(\hat{\tau}_{\lambda_i}, \tau_{\theta_j})\}_{i=1,j=1}^{N_\lambda,N_\theta}$, $\{(\tau_{\lambda_i}, \hat{\tau}_{\theta_j})\}_{i=1,j=0}^{N_\lambda,N_\theta}$, and $\{(\tau_{\lambda_i}, \tau_{\theta_j})\}_{i=1,j=1}^{N_\lambda,N_\theta}$, respectively, and applying Theorem 3, we get

$$\begin{aligned} U_I^{n+1}(\hat{\tau}_{\lambda_i}, \tau_{\theta_j}) + \left(\frac{\Delta t}{2R^2}\right) \Big[c(\tau_{\theta_j}) D_\lambda \phi_I^{n+1}(\hat{\tau}_{\lambda_i}, \tau_{\theta_j}) + d(\tau_{\theta_j}) \cos \tilde{\tau}_{\theta_j}^{n+\frac{1}{2}} D_\theta \phi_I^{n+1}(\hat{\tau}_{\lambda_i}, \tau_{\theta_j})\Big] \\ = \tilde{R}_u^n(\hat{\tau}_{\lambda_i}, \tau_{\theta_j}) + \varepsilon_u^{n+1}(\hat{\tau}_{\lambda_i}, \tau_{\theta_j}), \end{aligned} \tag{32}$$

$$
\begin{aligned}
V_I^{n+1}(\tau_{\lambda_i}, \hat{\tau}_{\theta_j}) + \left(\frac{\Delta t}{2R^2}\right) \left[-d(\hat{\tau}_{\theta_j}) D_\lambda \phi_I^{n+1}(\tau_{\lambda_i}, \hat{\tau}_{\theta_j}) + c(\hat{\tau}_{\theta_j}) \cos \tilde{\hat{\tau}}_{\theta_j}^{n+\frac{1}{2}} D_\theta \phi_I^{n+1}(\tau_{\lambda_i}, \hat{\tau}_{\theta_j})\right] \\
= \tilde{R}_v^n(\tau_{\lambda_i}, \hat{\tau}_{\theta_j}) + \varepsilon_v^{n+1}(\tau_{\lambda_i}, \hat{\tau}_{\theta_j}), \qquad (33)
\end{aligned}
$$

$$
\begin{aligned}
\cos \tilde{\tau}_{\theta_j}^{n+\frac{1}{2}} \zeta_I^{n+1}(\tau_{\lambda_i}, \tau_{\theta_j}) + \left(\frac{\Delta t}{2}\right) \left[\left(\frac{1}{\cos \tilde{\tau}_{\theta_j}^{n+\frac{1}{2}}}\right) D_\lambda U_I^{n+1}(\tau_{\lambda_i}, \tau_{\theta_j}) + D_\theta V_I^{n+1}(\tau_{\lambda_i}, \tau_{\theta_j})\right] \\
= \tilde{R}_\phi^n(\tau_{\lambda_i}, \tau_{\theta_j}) + \varepsilon_\phi^{n+1}(\tau_{\lambda_i}, \tau_{\theta_j}), \qquad (34)
\end{aligned}
$$

where ϵ_u^{n+1}, ϵ_v^{n+1}, and ϵ_ϕ^{n+1} are residual functions, derived later in this section. The points $\tilde{\tau}_{\theta_j}^{n+\frac{1}{2}}$ and $\tilde{\hat{\tau}}_{\theta_j}^{n+\frac{1}{2}}$ are defined by $\tilde{\tau}_{\theta_j}^{n+\frac{1}{2}} \equiv (\tau_{\theta_j} + \tilde{\tau}_{\theta_j})/2$ and $\tilde{\hat{\tau}}_{\theta_j}^{n+\frac{1}{2}} \equiv (\hat{\tau}_{\theta_j} + \tilde{\hat{\tau}}_{\theta_j})/2$, respectively, where $\tilde{\tau}_{\theta_j}$ and $\tilde{\hat{\tau}}_{\theta_j}$ are defined as the latitudinal positions at t_n of fluid particles whose trajectories have latitudinal positions of τ_{θ_j} and $\hat{\tau}_{\theta_j}$, respectively, at t_{n+1}.

To derive an expression for ε_u^{n+1} at $\{(\hat{\tau}_{\lambda_i}, \tau_{\theta_j})\}_{i=1,j=1}^{N_\lambda,N_\theta}$, we note that the second-order residual terms in ε_u^{n+1} arise from terms associated with the derivatives of the interpolant ϕ_I^{n+1}, namely, $(\frac{\Delta t}{2R^2}) c D_\lambda \phi_I^{n+1}$ and $(\frac{\Delta t}{2R^2}) d \cos \tilde{\tau}_{\theta_j}^{n+\frac{1}{2}} D_\theta \phi_I^{n+1}$. We first consider the former. Since (32) is collocated at $\{(\hat{\tau}_{\lambda_i}, \tau_{\theta_j})\}_{i=1,j=1}^{N_\lambda,N_\theta}$, which align in the λ-dimension with the gridpoints of Δ_3, the partition on which ϕ_I^{n+1} is defined, the second-order residual term associated with $(\frac{\Delta t}{2R^2}) c D_\lambda \phi_I^{n+1}$ is given by (28) in Theorem 3 as $-\left(\frac{\Delta t}{2R^2}\right) \frac{\Delta\lambda^2}{12} c D_\lambda^3 \phi^{n+1}$. In contrast, the collocation points $\{(\hat{\tau}_{\lambda_i}, \tau_{\theta_j})\}_{i=1,j=1}^{N_\lambda,N_\theta}$ align with the midpoints (not gridpoints) of Δ_3 in the θ-dimension. Therefore, the second-order residual term associated with $(\frac{\Delta t}{2R^2}) d \cos \tilde{\tau}_{\theta_j}^{n+\frac{1}{2}} D_\theta \phi_I^{n+1}$ is given by (24) in Theorem 3 as $\left(\frac{\Delta t}{2R^2}\right) \frac{\Delta\theta^2}{24} d \cos \tilde{\tau}_{\theta_j}^{n+\frac{1}{2}} D_\theta^3 \phi^{n+1}$. Combining these results, we obtain that at $\{(\hat{\tau}_{\lambda_i}, \tau_{\theta_j})\}_{i=1,j=1}^{N_\lambda,N_\theta}$

$$
\begin{aligned}
\varepsilon_u^{n+1}(\hat{\tau}_{\lambda_i}, \tau_{\theta_j}) = -\left(\frac{\Delta t}{2R^2}\right) \Bigg[& \frac{\Delta\lambda^2}{12} c(\tau_{\theta_j}) D_\lambda^3 \phi^{n+1}(\hat{\tau}_{\lambda_i}, \tau_{\theta_j}) \\
& - \frac{\Delta\theta^2}{24} d(\tau_{\theta_j}) \cos \tilde{\tau}_{\theta_j}^{n+\frac{1}{2}} D_\theta^3 \phi^{n+1}(\hat{\tau}_{\lambda_i}, \tau_{\theta_j}) + \mathcal{O}(h^4) \Bigg], \qquad (35)
\end{aligned}
$$

where $h \equiv \max\{\Delta\lambda, \Delta\theta\}$. Similarly, the residuals ε_v^{n+1} at $\{(\tau_{\lambda_i}, \hat{\tau}_{\theta_j})\}_{i=1,j=1}^{N_\lambda,N_\theta-1}$ and ε_ϕ^{n+1} at $\{(\tau_{\lambda_i}, \tau_{\theta_j})\}_{i=1,j=1}^{N_\lambda,N_\theta}$ are given by

$$
\begin{aligned}
\varepsilon_v^{n+1}(\tau_{\lambda_i}, \hat{\tau}_{\theta_j}) = -\left(\frac{\Delta t}{2R^2}\right) \Bigg[& -\frac{\Delta\lambda^2}{24} d(\hat{\tau}_{\theta_j}) \left(-D_\lambda^3 \phi^{n+1}(\tau_{\lambda_i}, \hat{\tau}_{\theta_j})\right) \\
& + \frac{\Delta\theta^2}{12} c(\hat{\tau}_{\theta_j}) \cos \tilde{\hat{\tau}}_{\theta_j}^{n+\frac{1}{2}} D_\theta^3 \phi^{n+1}(\tau_{\lambda_i}, \hat{\tau}_{\theta_j}) + \mathcal{O}(h^4) \Bigg], \qquad (36)
\end{aligned}
$$

$$\varepsilon_\phi^{n+1}(\tau_{\lambda_i},\tau_{\theta_j}) = -\left(\frac{\Delta t}{2}\right)\left[\frac{\Delta\lambda^2}{12}\frac{1}{\cos\tilde{\tau}_{\theta_j}^{n+\frac{1}{2}}}D_\lambda^3 U^{n+1}(\tau_{\lambda_i},\tau_{\theta_j}) \right.$$
$$\left. + \frac{\Delta\theta^2}{12}D_\theta^3 V^{n+1}(\tau_{\lambda_i},\tau_{\theta_j}) + \mathcal{O}(h^4)\right]. \quad (37)$$

At $\{(\tau_{\lambda_i},\hat{\tau}_{\theta_0}),(\tau_{\lambda_i},\hat{\tau}_{\theta_{N_\theta}})\}_{i=1}^{N_\lambda}$, the residual ε_v^{n+1} takes on a slightly different form

$$\varepsilon_v^{n+1}(\tau_{\lambda_i},\hat{\tau}_{\theta_j}) = -\left(\frac{\Delta t}{2R^2}\right)\left[-\frac{\Delta\lambda^2}{24}d(\hat{\tau}_{\theta_j})\left(-D_\lambda^3\phi^{n+1}(\tau_{\lambda_i},\hat{\tau}_{\theta_j})\right)\right.$$
$$\left. -\frac{\Delta\theta^2}{24}c(\hat{\tau}_{\theta_j})\cos\tilde{\tilde{\tau}}_{\theta_j}^{n+\frac{1}{2}}D_\theta^3\phi^{n+1}(\tau_{\lambda_i},\hat{\tau}_{\theta_j}) + \mathcal{O}(h^4)\right], \quad (38)$$

for $j = 0$ and $j = N_\theta$, because $\hat{\tau}_{\theta_0}$ and $\hat{\tau}_{\theta_{N_\theta}}$ are gridpoints of $\hat{\Delta}_\theta$ (alternatively, midpoints of Δ_θ) whereas $\{\hat{\tau}_{\theta_j}\}_{j=1}^{N_\theta-1}$ are midpoints of $\hat{\Delta}_\theta$ (alternatively, gridpoints of Δ_θ). According to Theorem 3, this implies that the coefficients of the perturbation terms associated with $D_\theta\phi_I^{n+1}$ are different in the two cases.

The derivatives of the interpolants of the geopotential ϕ^{n+1} and its logarithm satisfy

$$D_\theta\phi_I^{n+1}\left(\tau_{\lambda_i},\pm\frac{\pi}{2}\right) = -\frac{\Delta\theta^2}{12}D_\theta^3\phi^{n+1}\left(\tau_{\lambda_i},\pm\frac{\pi}{2}\right) + \mathcal{O}(h^4), \quad (39)$$
$$D_\theta\zeta_I^{n+1}\left(\tau_{\lambda_i},\pm\frac{\pi}{2}\right) = -\frac{\Delta\theta^2}{12}D_\theta^3\zeta^{n+1}\left(\tau_{\lambda_i},\pm\frac{\pi}{2}\right) + \mathcal{O}(h^4), \quad (40)$$

at the poles, for $i = 1,\dots,N_\lambda$, since $D_\theta\phi^{n+1}(\tau_{\lambda_i},\pm\pi/2) = 0$ and $D_\theta\zeta^{n+1}(\tau_{\lambda_i},\pm\pi/2) = 0$.

In order to derive a method with optimal convergence, the second-order terms in the residuals (35)–(38) and the boundary residuals (39) and (40) need to be eliminated. This is done by approximating the third derivatives to second-order accuracy using the spline interpolants, then using these approximations to eliminate the second-order terms.

Relations (26) and (29) give approximations to the third derivatives of a target function on the unstaggered partitions Δ_θ and Δ_λ. For the staggered partition $\hat{\Delta}_\theta$, where the first and last collocation points are gridpoints, we define another difference operator $\hat{\Lambda}'_\theta$ by

$$(\hat{\Lambda}'_\theta\psi)_{i,0} \equiv \frac{5\psi_{i,1} - 13\psi_{i,2} + 11\psi_{i,3} - 3\psi_{i,4}}{2\Delta\theta^2},$$

$$
\begin{aligned}
(\hat{\Lambda}'_\theta\psi)_{i,1} &\equiv \frac{2\psi_{i,1} - 5\psi_{i,2} + 4\psi_{i,3} - \psi_{i,4}}{\Delta\theta^2}, \\
(\hat{\Lambda}'_\theta\psi)_{i,j} &\equiv \frac{\psi_{i,j-1} - 2\psi_{i,j} + \psi_{i,j+1}}{\Delta\theta^2}, \qquad j = 2, \ldots, N_\theta - 2, \\
(\hat{\Lambda}'_\theta\psi)_{i,N_\theta-1} &\equiv \frac{2\psi_{i,N_\theta-1} - 5\psi_{i,N_\theta-2} + 4\psi_{i,N_\theta-3} - \psi_{i,N_\theta-4}}{\Delta\theta^2}, \\
(\hat{\Lambda}'_\theta\psi)_{i,N_\theta} &\equiv \frac{5\psi_{i,N_\theta-1} - 13\psi_{i,N_\theta-2} + 11\psi_{i,N_\theta-3} - 3\psi_{i,N_\theta-4}}{2\Delta\theta^2},
\end{aligned}
$$

for $i = 1, \ldots, N_\lambda$, and where the second subscript refers to the staggered collocation points $\{\hat{\tau}_{\theta_j}\}_{j=0}^{N_\theta}$. For the staggered collocation points in the λ direction we do not need to define a new operator, since periodicity introduces significant simplification. We simply extend the definition of Λ'_λ to apply to staggered collocation points, by allowing the first subscript in (21) to refer to either the staggered or the unstaggered collocation points $\{\hat{\tau}_{\lambda_i}\}_{i=1}^{i=N_\lambda}$ and $\{\tau_{\lambda_i}\}_{i=1}^{i=N_\lambda}$.

From the results in Theorem 3, the third derivatives of ϕ^{n+1}, for instance, can be approximated to second order using the first derivative of its interpolant ϕ_I^{n+1} and the above difference operators. More specifically, $D_\lambda^3\phi^{n+1}$ and $D_\theta^3\phi^{n+1}$ can be approximated at the collocation points of Δ_1 using $D_\lambda\phi_I^{n+1}$ and $D_\theta\phi_I^{n+1}$, respectively, by

$$
\begin{aligned}
(D_\lambda^3\phi^{n+1})(\hat{\tau}_{\lambda_i}, \tau_{\theta_j}) &= (\Lambda'_\lambda(D_\lambda\phi_I^{n+1}))(\hat{\tau}_{\lambda_i}, \tau_{\theta_j}) + \mathcal{O}(\Delta\lambda^2), \\
(D_\theta^3\phi^{n+1})(\hat{\tau}_{\lambda_i}, \tau_{\theta_j}) &= (\Lambda'_\theta(D_\theta\phi_I^{n+1}))(\hat{\tau}_{\lambda_i}, \tau_{\theta_j}) + \mathcal{O}(\Delta\theta^2),
\end{aligned}
$$

for $i = 1, \ldots, N_\lambda$ and $j = 1, \ldots, N_\theta$. On the other hand, the difference operator $\hat{\Lambda}'_\theta$ and the interpolant V_I^{n+1} can be used to approximate $D_\theta^3 V^{n+1}$ at the collocation points of Δ_2 by

$$
(D_\theta^3 V^{n+1})(\tau_{\lambda_i}, \hat{\tau}_{\theta_j}) = (\hat{\Lambda}'_\theta(D_\theta V_I^{n+1}))(\tau_{\lambda_i}, \hat{\tau}_{\theta_j}) + \mathcal{O}(\Delta\theta^2),
$$

for $i = 1, \ldots, N_\lambda$ and $j = 0, \ldots, N_\theta$. Similar relations hold for the other functions, leading to fourth-order approximations for the residuals of (35)–(38) at the collocation points of Δ_1, Δ_2 and Δ_3, respectively, given by

$$
\begin{aligned}
\varepsilon_u^{n+1}(\hat{\tau}_{\lambda_i}, \tau_{\theta_j}) = -\left(\frac{\Delta t}{2R^2}\right) \Bigg[&\frac{\Delta\lambda^2}{12} c(\tau_{\theta_j}) \left(\Lambda'_\lambda(D_\lambda\phi_I^{n+1})\right)(\hat{\tau}_{\lambda_i}, \tau_{\theta_j}) \\
&- \frac{\Delta\theta^2}{24} d(\tau_{\theta_j}) \cos\tilde{\tau}_{\theta_j}^{n+\frac{1}{2}} \left(\Lambda'_\theta(D_\theta\phi_I^{n+1})\right)(\hat{\tau}_{\lambda_i}, \tau_{\theta_j}) + \mathcal{O}(h^4) \Bigg],
\end{aligned}
\tag{41}
$$

for $i = 1, \dots, N_\lambda$ and $j = 1, \dots, N_\theta$,

$$\begin{aligned}\varepsilon_v^{n+1}(\tau_{\lambda_i}, \hat{\tau}_{\theta_j}) = -\left(\frac{\Delta t}{2R^2}\right)\Bigg[&-\frac{\Delta\lambda^2}{24} d(\hat{\tau}_{\theta_j})\left(\Lambda'_\lambda(-D_\lambda \phi_I^{n+1})\right)(\tau_{\lambda_i}, \hat{\tau}_{\theta_j}) \\ &+\frac{\Delta\theta^2}{12} c(\hat{\tau}_{\theta_j}) \cos \tilde{\hat{\tau}}_{\theta_j}^{n+\frac{1}{2}}\left(\hat{\Lambda}'_\theta(D_\theta \phi_I^{n+1})\right)(\tau_{\lambda_i}, \hat{\tau}_{\theta_j}) + \mathcal{O}(h^4)\Bigg],\end{aligned} \tag{42}$$

for $i = 1, \dots, N_\lambda$ and $j = 1, \dots, N_\theta - 1$,

$$\begin{aligned}\varepsilon_\phi^{n+1}(\tau_{\lambda_i}, \tau_{\theta_j}) = -\left(\frac{\Delta t}{2}\right)\Bigg[&\frac{\Delta\lambda^2}{12} \frac{1}{\cos \tilde{\tau}_{\theta_j}^{n+\frac{1}{2}}}\left(\Lambda'_\lambda(D_\lambda U_I^{n+1})\right)(\tau_{\lambda_i}, \tau_{\theta_j}) \\ &+\frac{\Delta\theta^2}{12}\left(\Lambda'_\theta(D_\theta V_I^{n+1})\right)(\tau_{\lambda_i}, \tau_{\theta_j}) + \mathcal{O}(h^4)\Bigg],\end{aligned} \tag{43}$$

for $i = 1, \dots, N_\lambda$ and $j = 1, \dots, N_\theta$,

$$\begin{aligned}\varepsilon_v^{n+1}(\tau_{\lambda_i}, \hat{\tau}_{\theta_j}) = -\left(\frac{\Delta t}{2R^2}\right)\Bigg[&-\frac{\Delta\lambda^2}{24} d(\hat{\tau}_{\theta_j})\left(\Lambda'_\lambda(-D_\lambda \phi_I^{n+1})\right)(\tau_{\lambda_i}, \hat{\tau}_{\theta_j}) \\ &-\frac{\Delta\theta^2}{24} c(\hat{\tau}_{\theta_j}) \cos \tilde{\hat{\tau}}_{\theta_j}^{n+\frac{1}{2}}\left(\hat{\Lambda}'_\theta(D_\theta \phi_I^{n+1})\right)(\tau_{\lambda_i}, \hat{\tau}_{\theta_j}) + \mathcal{O}(h^4)\Bigg],\end{aligned} \tag{44}$$

for $i = 1, \dots, N_\lambda$ and $j = 0, N_\theta$.

The above equations allow us to eliminate the second-order terms of the residuals in (32)–(34) and to obtain higher-order solutions, as will be explained in the rest of this section.

2.2 The One-Step Optimal Quadratic Spline Collocation Method

In the one-step method, the second-order perturbation terms inside the square brackets in (41)–(44) are combined with the associated derivative operators to form "perturbed operators," which are then incorporated into the system to yield a higher-order approximation. For example, the first perturbation term inside the square brackets of (41), $\frac{\Delta\lambda^2}{12} c\Lambda'_\lambda(D_\lambda \phi_I^{n+1})$, arises from the second term on the left side of (32), $cD_\lambda \phi_I^{n+1}$. These two terms can therefore be combined to form

$$c\left(I + \frac{\Delta\lambda^2}{12}\Lambda'_\lambda\right) D_\lambda \phi_I^{n+1},$$

where I denotes the identity operator. This motivates us to define the perturbed operator

$$D_\lambda'^{\Delta\to\hat{\Delta}} \equiv \left(I + \frac{\Delta\lambda^2}{12}\Lambda_\lambda'\right) D_\lambda,$$

where the superscript $\Delta \to \hat{\Delta}$ indicates that the perturbed derivative values at collocation points in $\hat{\Delta}_\lambda$ are computed from spline coefficients defined with respect to Δ_λ. Similarly, the first perturbation term inside the square brackets of (43), $\frac{\Delta\lambda^2}{12}\frac{1}{\cos\tilde{\tau}_{\theta_j}^{n+\frac{1}{2}}}\Lambda_\lambda'(D_\lambda U_I^{n+1})$, arises from the second term on the left side of (34), $\frac{1}{\cos\tilde{\tau}_{\theta_j}^{n+\frac{1}{2}}} D_\lambda U_I^{n+1}$. Combining these two terms gives

$$\frac{1}{\cos\tilde{\tau}_{\theta_j}^{n+\frac{1}{2}}}\left(I + \frac{\Delta\lambda^2}{12}\Lambda_\lambda'\right) D_\lambda U_I^{n+1} \equiv \frac{1}{\cos\tilde{\tau}_{\theta_j}^{n+\frac{1}{2}}} D_\lambda'^{\hat{\Delta}\to\Delta} U_I^{n+1}.$$

To simplify the notation, we define

$$D_\lambda'^{\to} \equiv \left(I + \frac{\Delta\lambda^2}{12}\Lambda_\lambda'\right) D_\lambda = D_\lambda'^{\Delta\to\hat{\Delta}} = D_\lambda'^{\hat{\Delta}\to\Delta},$$

where the arrow indicates that $D_\lambda'^{\to}$ computes the perturbed derivative values at collocation points in $\hat{\Delta}_\lambda$ from spline coefficients defined with respect to Δ_λ, or vice versa. Furthermore, combining the term $-\frac{\Delta\theta^2}{24} d\cos\tilde{\tau}_{\theta_j}^{n+\frac{1}{2}}\Lambda_\theta'(D_\theta\phi_I^{n+1})$ of (41) with $d\cos\tilde{\tau}_{\theta_j}^{n+\frac{1}{2}} D_\theta\phi_I^{n+1}$ of (32), the term $-\frac{\Delta\lambda^2}{24} d\Lambda_\lambda'(D_\lambda\phi_I^{n+1})$ of (42) with $dD_\lambda\phi_I^{n+1}$ of (33), and the term $\frac{\Delta\theta^2}{12}\Lambda_\theta'(D_\theta V_I^{n+1})$ of (43) with $D_\theta V_I^{n+1}$ of (34), we obtain

$$d\cos\tilde{\tau}_{\theta_j}^{n+\frac{1}{2}}\left(I - \frac{\Delta\theta^2}{24}\Lambda_\theta'\right) D_\theta\phi_I^{n+1},\ d\left(I - \frac{\Delta\lambda^2}{24}\Lambda_\lambda'\right) D_\lambda\phi_I^{n+1},\ \left(I + \frac{\Delta\theta^2}{12}\Lambda_\theta'\right) D_\theta V_I^{n+1},$$

respectively. Thus, we define the following perturbed operators:

$$D_\theta' \equiv \left(I - \frac{\Delta\theta^2}{24}\Lambda_\theta'\right) D_\theta,\ \ D_\lambda' \equiv \left(I - \frac{\Delta\lambda^2}{24}\Lambda_\lambda'\right) D_\lambda,\ \ D_\theta'^{\hat{\Delta}\to\Delta} \equiv \left(I + \frac{\Delta\theta^2}{12}\Lambda_\theta'\right) D_\theta.$$

The perturbed operator $D_\theta'^{\Delta\to\hat{\Delta}}$, which computes first derivative values in the θ-direction and the associated residual terms on the $\hat{\Delta}_\theta$-grid, needs to be defined carefully because, as noted before, the residual terms for the collocation points $\{(\tau_{\lambda_i}, \hat{\tau}_{\theta_0}), (\tau_{\lambda_i}, \hat{\tau}_{\theta_{N_\theta}})\}_{i=1}^{N_\lambda}$ are slightly different from the rest. At $\{(\tau_{\lambda_i}, \hat{\tau}_{\theta_j})\}_{i=1,j=1}^{N_\lambda, N_\theta-1}$, the residual term associated with $c\cos\hat{\tilde{\tau}}_{\theta_j}^{n+\frac{1}{2}} D_\theta\phi_I^{n+1}$ is $\frac{\Delta\theta^2}{12} c\cos\hat{\tilde{\tau}}_{\theta_j}^{n+\frac{1}{2}}\hat{\Lambda}_\theta'\Delta_\theta\phi_I^{n+1}$ in (42), whereas at $\{(\tau_{\lambda_i}, \hat{\tau}_{\theta_0}), (\tau_{\lambda_i}, \hat{\tau}_{\theta_{N_\theta}})\}_{i=1}^{N_\lambda}$

the respective term is given by
$-\frac{\Delta\theta^2}{24}c\cos\tilde{\hat{\tau}}_{\theta_j}^{n+\frac{1}{2}}\hat{\Lambda}'_\theta\Delta_\theta\phi_I^{n+1}$ in (44). Therefore, we define $D_\theta^{'\Delta\to\hat{\Delta}}$ at $\{(\tau_{\lambda_i},\hat{\tau}_{\theta_j})\}_{i=1,j=1}^{N_\lambda,N_\theta-1}$ by

$$(D_\theta^{'\Delta\to\hat{\Delta}}u)(\tau_{\lambda_i},\hat{\tau}_{\theta_j}) \equiv \left[\left(I+\frac{\Delta\theta^2}{12}\hat{\Lambda}'_\theta\right)(D_\theta u)\right](\tau_{\lambda_i},\hat{\tau}_{\theta_j}),$$

and at $\{(\tau_{\lambda_i},\hat{\tau}_{\theta_0}),(\tau_{\lambda_i},\hat{\tau}_{\theta_{N_\theta}})\}_{i=1}^{N_\lambda}$ by

$$(D_\theta^{'\Delta\to\hat{\Delta}}u)(\tau_{\lambda_i},\hat{\tau}_{\theta_j}) \equiv \left[\left(I-\frac{\Delta\theta^2}{24}\hat{\Lambda}'_\theta\right)(D_\theta u)\right](\tau_{\lambda_i},\hat{\tau}_{\theta_j}),$$

for $j=0, N_\theta$.

Having defined the perturbed operators, we can derive the one-step OQSC method. In the one-step method, we determine the approximations U_Δ^{n+1}, V_Δ^{n+1}, and ϕ_Δ^{n+1} by solving

$$\begin{aligned}
U_\Delta^{n+1}(\hat{\tau}_{\lambda_i},\tau_{\theta_j})+&\left(\frac{\Delta t}{2R^2}\right)\left[c(\tau_{\theta_j})D_\lambda^{'\to}\phi_\Delta^{n+1}(\hat{\tau}_{\lambda_i},\tau_{\theta_j})+d(\tau_{\theta_j})\cos\tilde{\tau}_{\theta_j}^{n+\frac{1}{2}}D'_\theta\phi_\Delta^{n+1}(\hat{\tau}_{\lambda_i},\tau_{\theta_j})\right]\\
=&\tilde{R}_u^{'n}(\hat{\tau}_{\lambda_i},\tau_{\theta_j}), \qquad (45)\\
V_\Delta^{n+1}(\tau_{\lambda_i},\hat{\tau}_{\theta_j})+&\left(\frac{\Delta t}{2R^2}\right)\left[-d(\hat{\tau}_{\theta_j})D'_\lambda\phi_\Delta^{n+1}(\tau_{\lambda_i},\tau_{\theta_j})+c(\hat{\tau}_{\theta_j})\cos\tilde{\hat{\tau}}_{\theta_j}^{n+\frac{1}{2}}D_\theta^{'\Delta\to\hat{\Delta}}\phi_\Delta^{n+1}(\tau_{\lambda_i},\tau_{\theta_j})\right]\\
=&\tilde{R}_v^{'n}(\tau_{\lambda_i},\hat{\tau}_{\theta_j}), \qquad (46)\\
\cos\tilde{\tau}_{\theta_j}^{n+\frac{1}{2}}\zeta_\Delta^{n+1}(\tau_{\lambda_i},\tau_{\theta_j})+&\left(\frac{\Delta t}{2}\right)\left[\left(\frac{1}{\cos\tilde{\tau}_{\theta_j}^{n+\frac{1}{2}}}\right)D_\lambda^{'\to}U^{n+1}(\tau_{\lambda_i},\tau_{\theta_j})+D_\theta^{'\hat{\Delta}\to\Delta}V^{n+1}(\tau_{\lambda_i},\tau_{\theta_j})\right]\\
=&\tilde{R}_\phi^{'n}(\tau_{\lambda_i},\tau_{\theta_j}), \qquad (47)
\end{aligned}$$

at $\{(\hat{\tau}_{\lambda_i},\tau_{\theta_j})\}_{i=1,j=1}^{N_\lambda,N_\theta}$, $\{(\tau_{\lambda_i},\hat{\tau}_{\theta_j})\}_{i=1,j=0}^{N_\lambda,N_\theta}$, and $\{(\tau_{\lambda_i},\tau_{\theta_j})\}_{i=1,j=1}^{N_\lambda,N_\theta}$, respectively, where

$$\begin{aligned}
\tilde{R}_u^{'n}(\hat{\tau}_{\lambda_i},\tau_{\theta_j}) =\ & a(\tau_{\theta_j})U_\Delta^n(\tilde{\hat{\tau}}_{\lambda_i},\tilde{\tau}_{\theta_j})+b(\tau_{\theta_j})V_\Delta^n(\tilde{\hat{\tau}}_{\lambda_i},\tilde{\tau}_{\theta_j}) \qquad (48)\\
&-\left(\frac{\Delta t}{2R^2}\right)\left[c(\tau_{\theta_j})D_\lambda^{'\to}\phi_\Delta^n(\tilde{\hat{\tau}}_{\lambda_i},\tilde{\tau}_{\theta_j})+d(\tau_{\theta_j})\cos\tilde{\tau}_{\theta_j}^{n+\frac{1}{2}}D'_\theta\phi_\Delta^n(\tilde{\hat{\tau}}_{\lambda_i},\tilde{\tau}_{\theta_j})\right]\\
&-\Delta t d(\tau_{\theta_j})\tilde{\delta}_\Delta^{n+\frac{1}{2}}(\hat{\tau}_{\lambda_i},\tau_{\theta_j}),\\
\tilde{R}_v^{'n}(\tau_{\lambda_i},\hat{\tau}_{\theta_j}) =& -b(\hat{\tau}_{\theta_j})U_\Delta^n(\tilde{\tau}_{\lambda_i},\tilde{\hat{\tau}}_{\theta_j})+a(\hat{\tau}_{\theta_j})V_\Delta^n(\tilde{\tau}_{\lambda_i},\tilde{\hat{\tau}}_{\theta_j}) \qquad (49)\\
&-\left(\frac{\Delta t}{2R^2}\right)\left[-d(\hat{\tau}_{\theta_j})D'_\lambda\phi_\Delta^n(\tilde{\tau}_{\lambda_i},\tilde{\hat{\tau}}_{\theta_j})+c(\hat{\tau}_{\theta_j})\cos\tilde{\hat{\tau}}_{\theta_j}^{n+\frac{1}{2}}D_\theta^{'\Delta\to\hat{\Delta}}\phi_\Delta^n(\tilde{\tau}_{\lambda_i},\tilde{\hat{\tau}}_{\theta_j})\right]\\
&-\Delta t c(\hat{\tau}_{\theta_j})\tilde{\delta}_\Delta^{n+\frac{1}{2}}(\tau_{\lambda_i},\hat{\tau}_{\theta_j}),\\
\tilde{R}_\phi^{'n}(\tau_{\lambda_i},\tau_{\theta_j}) =& \cos\tilde{\tau}_{\theta_j}^{n+\frac{1}{2}}\zeta_\Delta^n(\tilde{\tau}_{\lambda_i},\tilde{\tau}_{\theta_j}) \qquad (50)
\end{aligned}$$

$$- \left(\frac{\Delta t}{2}\right) \left[\left(\frac{1}{\cos \tilde{\tau}_{\theta_j}^{n+\frac{1}{2}}} \right) D_\lambda^{'\to} U_\Delta^n(\tilde{\tau}_{\lambda_i}, \tilde{\tau}_{\theta_j}) + D_\theta^{'\hat{\Delta}\to\Delta} V_\Delta^n(\tilde{\tau}_{\lambda_i}, \tilde{\tau}_{\theta_j}) \right].$$

and $\delta_\Delta^{n+\frac{1}{2}} \equiv \left((U_\Delta^{n+\frac{1}{2}})^2 + (V_\Delta^{n+\frac{1}{2}})^2 \right) \sin \theta^{n+\frac{1}{2}} / \cos^2 \theta^{n+\frac{1}{2}}$. The points $\tilde{\tau}_{\lambda_i}$ and $\tilde{\hat{\tau}}_{\lambda_i}$ are defined as the longitudinal positions at t_n of fluid particles whose trajectories have longitudinal positions of τ_{λ_i} and $\hat{\tau}_{\lambda_i}$, respectively, at t_{n+1}. Recall also from subsection 2.1 that the points $\tilde{\tau}_{\theta_j}$ and $\tilde{\hat{\tau}}_{\theta_j}$ were defined as the latitudinal counterparts of $\tilde{\tau}_{\lambda_i}$ and $\tilde{\hat{\tau}}_{\lambda_i}$, respectively.

In addition, the biquadratic splines U_Δ^{n+1}, V_Δ^{n+1}, ϕ_Δ^{n+1}, and ζ_Δ^{n+1} satisfy periodic conditions in the longitudinal dimension, and the latitudinal boundary conditions

$$\begin{aligned} &U_\Delta^{n+1}(\hat{\tau}_{\lambda_i}, \pm\tfrac{\pi}{2}) = 0, && V_\Delta^{n+1}(\tau_{\lambda_i}, \pm\tfrac{\pi}{2}) = 0, \\ &D_\theta^{'\hat{\Delta}\to\Delta}\phi_\Delta^{n+1}(\tau_{\lambda_i}, \pm\tfrac{\pi}{2}) = 0, && D_\theta^{'\hat{\Delta}\to\Delta}\zeta_\Delta^{n+1}(\tau_{\lambda_i}, \pm\tfrac{\pi}{2}) = 0, \end{aligned} \tag{51}$$

for $i = 1, \ldots, N_\lambda$.

The divergence terms are eliminated from (47) using (45) and (46); the resulting Helmholtz equation is then linearized and solved using fixed-point iteration. In Section 3, we report results of numerical experiments that show that the approximations have fourth-order errors at midpoints, which are optimal for quadratic splines.

2.3 The Two-Step Optimal Quadratic Spline Collocation Method

Alternatively, the two-step optimal quadratic spline collocation method can be used. In the first step, the biquadratic splines $\breve{U}_\Delta^{n+1}$, $\breve{V}_\Delta^{n+1}$, and $\breve{\phi}_\Delta^{n+1}$, which satisfy

$$\begin{aligned} \breve{U}_\Delta^{n+1}(\hat{\tau}_{\lambda_i}, \tau_{\theta_j}) &+ \left(\frac{\Delta t}{2R^2}\right) \left[c(\tau_{\theta_j}) D_\lambda \breve{\phi}_\Delta^{n+1}(\hat{\tau}_{\lambda_i}, \tau_{\theta_j}) + d(\tau_{\theta_j}) \cos \tilde{\tau}_{\theta_j}^{n+\frac{1}{2}} D_\theta \breve{\phi}_\Delta^{n+1}(\hat{\tau}_{\lambda_i}, \tau_{\theta_j}) \right] \\ &= \tilde{R}_{\breve{u}}^{'n}(\hat{\tau}_{\lambda_i}, \tau_{\theta_j}), \end{aligned} \tag{52}$$

$$\begin{aligned} \breve{V}_\Delta^{n+1}(\tau_{\lambda_i}, \hat{\tau}_{\theta_j}) &+ \left(\frac{\Delta t}{2R^2}\right) \left[-d(\hat{\tau}_{\theta_j}) D_\lambda \breve{\phi}_\Delta^{n+1}(\tau_{\lambda_i}, \hat{\tau}_{\theta_j}) + c(\hat{\tau}_{\theta_j}) \cos \tilde{\hat{\tau}}_{\theta_j}^{n+\frac{1}{2}} D_\theta \breve{\phi}_\Delta^{n+1}(\tau_{\lambda_i}, \hat{\tau}_{\theta_j}) \right] \\ &= \tilde{R}_{\breve{v}}^{'n}(\tau_{\lambda_i}, \hat{\tau}_{\theta_j}), \end{aligned} \tag{53}$$

$$\begin{aligned} \cos \tilde{\tau}_{\theta_j}^{n+\frac{1}{2}} \breve{\zeta}_\Delta^{n+1}(\tau_{\lambda_i}, \tau_{\theta_j}) &+ \left(\frac{\Delta t}{2}\right) \left[\left(\frac{1}{\cos \tilde{\tau}_{\theta_j}^{n+\frac{1}{2}}} \right) D_\lambda \breve{U}_\Delta^{n+1}(\tau_{\lambda_i}, \tau_{\theta_j}) + D_\theta \breve{V}_\Delta^{n+1}(\tau_{\lambda_i}, \tau_{\theta_j}) \right] \\ &= \tilde{R}_{\breve{\phi}}^{'n}(\tau_{\lambda_i}, \tau_{\theta_j}), \end{aligned} \tag{54}$$

at $\{(\hat{\tau}_{\lambda_i}, \tau_{\theta_j})\}_{i=1,j=1}^{N_\lambda,N_\theta}$, $\{(\tau_{\lambda_i}, \hat{\tau}_{\theta_j})\}_{i=1,j=0}^{N_\lambda,N_\theta}$, and $\{(\tau_{\lambda_i}, \tau_{\theta_j})\}_{i=1,j=1}^{N_\lambda,N_\theta}$, respectively, are determined. The right-side functions $\tilde{R}'^{n}_{\breve{u}}(\hat{\tau}_{\lambda_i}, \tau_{\theta_j})$, $\tilde{R}'^{n}_{\breve{v}}(\tau_{\lambda_i}, \hat{\tau}_{\theta_j})$ and $\tilde{R}'^{n}_{\breve{\phi}}(\tau_{\lambda_i}, \tau_{\theta_j})$ are defined similarly as $\tilde{R}'^{n}_{\breve{u}}(\hat{\tau}_{\lambda_i}, \tau_{\theta_j})$, $\tilde{R}'^{n}_{\breve{v}}(\tau_{\lambda_i}, \hat{\tau}_{\theta_j})$ and $\tilde{R}'^{n}_{\breve{\phi}}(\tau_{\lambda_i}, \tau_{\theta_j})$, respectively in (48)–(50), but with $\breve{U}^n_\Delta$, $\breve{V}^n_\Delta$, $\breve{\phi}^n_\Delta$, and $\breve{\zeta}^n_\Delta$ substituted in place of U^n_Δ, V^n_Δ, ϕ^n_Δ, and ζ^n_Δ, respectively. With the appropriate choice of basis functions as explained in Section 2.1, the biquadratic splines $\breve{U}^{n+1}_\Delta$, $\breve{V}^{n+1}_\Delta$, $\breve{\phi}^{n+1}_\Delta$, and $\breve{\zeta}^{n+1}_\Delta$ satisfy periodic conditions in the longitudinal dimension, and the latitudinal boundary conditions

$$\begin{aligned} &\breve{U}^{n+1}_\Delta(\hat{\tau}_{\lambda_i}, \pm\tfrac{\pi}{2}) = 0, &&\breve{V}^{n+1}_\Delta(\tau_{\lambda_i}, \pm\tfrac{\pi}{2}) = 0,\\ &D_\theta\breve{\phi}^{n+1}_\Delta(\tau_{\lambda_i}, \pm\tfrac{\pi}{2}) = 0, &&D_\theta\breve{\zeta}^{n+1}_\Delta(\tau_{\lambda_i}, \pm\tfrac{\pi}{2}) = 0, \end{aligned} \tag{55}$$

for $i = 1, \ldots, N_\lambda$. Thus, $\breve{U}^{n+1}_\Delta$, $\breve{V}^{n+1}_\Delta$, and $\breve{\phi}^{n+1}_\Delta$ are the solutions of the standard QSC method and are low-order approximations. In the two-step OQSC method, they are used to approximate the residual terms to fourth order. To this end, we define ε'^{n+1}_u, ε'^{n+1}_v, and ε'^{n+1}_ϕ at the associated collocation points as

$$\begin{aligned} \varepsilon'^{n+1}_u(\hat{\tau}_{\lambda_i}, \tau_{\theta_j}) = -\left(\frac{\Delta t}{2R^2}\right)\Bigg[&\frac{\Delta\lambda^2}{12}c(\tau_{\theta_j})\left(\Lambda'_\lambda(D_\lambda\breve{\phi}^{n+1}_\Delta)\right)(\hat{\tau}_{\lambda_i}, \tau_{\theta_j})\\ &-\frac{\Delta\theta^2}{24}d(\tau_{\theta_j})\cos\tilde{\tau}_\theta^{n+\frac{1}{2}}\left(\Lambda'_\theta(D_\theta\breve{\phi}^{n+1}_\Delta)\right)(\hat{\tau}_{\lambda_i}, \tau_{\theta_j})\Bigg], \end{aligned}$$

for $i = 1, \ldots, N_\lambda$ and $j = 1, \ldots, N_\theta$, (56)

$$\begin{aligned} \varepsilon'^{n+1}_v(\tau_{\lambda_i}, \hat{\tau}_{\theta_j}) = -\left(\frac{\Delta t}{2R^2}\right)\Bigg[&-\frac{\Delta\lambda^2}{24}d(\hat{\tau}_{\theta_j})\left(\Lambda'_\lambda(-D_\lambda\breve{\phi}^{n+1}_\Delta)\right)(\tau_{\lambda_i}, \hat{\tau}_{\theta_j})\\ &+\frac{\Delta\theta^2}{12}c(\hat{\tau}_{\theta_j})\cos\tilde{\hat{\tau}}_\theta^{n\frac{1}{2}}\left(\hat{\Lambda}'_\theta(D_\theta\breve{\phi}^{n+1}_\Delta)\right)(\tau_{\lambda_i}, \hat{\tau}_{\theta_j})\Bigg], \end{aligned}$$

for $i = 1, \ldots, N_\lambda$ and $j = 1, \ldots, N_\theta - 1$, (57)

$$\begin{aligned} \varepsilon'^{n+1}_\phi(\tau_{\lambda_i}, \tau_{\theta_j}) = -\left(\frac{\Delta t}{2}\right)\Bigg[&\frac{\Delta\lambda^2}{12}\frac{1}{\cos\tilde{\tau}_{\theta_j}^{n+\frac{1}{2}}}\left(\Lambda'_\lambda(D_\lambda\breve{U}^{n+1}_\Delta)\right)(\tau_{\lambda_i}, \tau_{\theta_j})\\ &+\frac{\Delta\theta^2}{12}\left(\Lambda'_\theta(D_\theta\breve{V}^{n+1}_\Delta)\right)(\tau_{\lambda_i}, \tau_{\theta_j})\Bigg], \end{aligned}$$

for $i = 1, \ldots, N_\lambda$ and $j = 1, \ldots, N_\theta$, (58)

$$\begin{aligned} \varepsilon'^{n+1}_v(\tau_{\lambda_i}, \hat{\tau}_{\theta_j}) = -\left(\frac{\Delta t}{2R^2}\right)\Bigg[&-\frac{\Delta\lambda^2}{24}d(\hat{\tau}_{\theta_j})\left(\Lambda'_\lambda(-D_\lambda\breve{\phi}^{n+1}_\Delta)\right)(\tau_{\lambda_i}, \hat{\tau}_{\theta_j})\\ &-\frac{\Delta\theta^2}{24}c(\hat{\tau}_{\theta_j})\cos\tilde{\hat{\tau}}_\theta^{n+\frac{1}{2}}\left(\hat{\Lambda}'_\theta(D_\theta\breve{\phi}^{n+1}_\Delta)\right)(\tau_{\lambda_i}, \hat{\tau}_{\theta_j})\Bigg], \end{aligned}$$

for $i = 1, \ldots, N_\lambda$ and $j = 0, N_\theta$. (59)

Similarly, the boundary residuals can also be estimated to fourth-order accuracy using the second-order approximation. To this end, we define

$$\begin{aligned} \gamma_\phi^{n+1}(\tau_{\lambda_i}, \tau_{\theta_j}) &= -\frac{\Delta\theta^2}{12}\Lambda'_\theta(D_\theta\breve{\phi}_\Delta^{n+1})(\tau_{\lambda_i}, \tau_{\theta_j}), && (60)\\ \gamma_\zeta^{n+1}(\tau_{\lambda_i}, \tau_{\theta_j}) &= -\frac{\Delta\theta^2}{12}\Lambda'_\theta(D_\theta\breve{\zeta}_\Delta^{n+1})(\tau_{\lambda_i}, \tau_{\theta_j}), && (61) \end{aligned}$$

where $i = 1, \ldots, N_\lambda$ and $j = 0, N_\theta + 1$.

In the second step, the terms $\varepsilon_u'^{n+1}$, $\varepsilon_v'^{n+1}$, and $\varepsilon_\phi'^{n+1}$ are added to the right sides of (52)–(54), and the biquadratic splines U_Δ^{n+1}, V_Δ^{n+1}, ϕ_Δ^{n+1}, and ζ_Δ^{n+1} are determined by solving the equations

$$\begin{aligned} &U_\Delta^{n+1}(\hat\tau_{\lambda_i}, \tau_{\theta_j}) + \left(\frac{\Delta t}{2R^2}\right)\left[c(\tau_{\theta_j})D_\lambda\phi_\Delta^{n+1}(\hat\tau_{\lambda_i}, \tau_{\theta_j}) + d(\tau_{\theta_j})\cos\tilde\tau_{\theta_j}^{n+\frac12}D_\theta\phi_\Delta^{n+1}(\hat\tau_{\lambda_i}, \tau_{\theta_j})\right]\\ &\qquad = \tilde R_u'^n(\hat\tau_{\lambda_i}, \tau_{\theta_j}) + \varepsilon_u'^{n+1}(\hat\tau_{\lambda_i}, \tau_{\theta_j}), && (62)\\ &V_\Delta^{n+1}(\tau_{\lambda_i}, \hat\tau_{\theta_j}) + \left(\frac{\Delta t}{2R^2}\right)\left[-d(\hat\tau_{\theta_j})D_\lambda\phi_\Delta^{n+1}(\tau_{\lambda_i}, \hat\tau_{\theta_j}) + c(\hat\tau_{\theta_j})\cos\tilde{\hat\tau}_{\theta_j}^{n+\frac12}D_\theta\phi_\Delta^{n+1}(\tau_{\lambda_i}, \hat\tau_{\theta_j})\right]\\ &\qquad = \tilde R_v'^n(\tau_{\lambda_i}, \hat\tau_{\theta_j}) + \varepsilon_v'^{n+1}(\tau_{\lambda_i}, \hat\tau_{\theta_j}), && (63)\\ &\cos\tilde\tau_{\theta_j}^{n+\frac12}\zeta_\Delta^{n+1}(\tau_{\lambda_i}, \tau_{\theta_j}) + \left(\frac{\Delta t}{2}\right)\left[\left(\frac{1}{\cos\tilde\tau_{\theta_j}^{n+\frac12}}\right)D_\lambda U_\Delta^{n+1}(\tau_{\lambda_i}, \tau_{\theta_j}) + D_\theta V_\Delta^{n+1}(\tau_{\lambda_i}, \tau_{\theta_j})\right]\\ &\qquad = \tilde R_\phi'^n(\tau_{\lambda_i}, \tau_{\theta_j}) + \varepsilon_\phi'^{n+1}(\tau_{\lambda_i}, \tau_{\theta_j}), && (64) \end{aligned}$$

at $\{(\hat\tau_{\lambda_i}, \tau_{\theta_j})\}_{i=1,j=1}^{N_\lambda,N_\theta}$, $\{(\tau_{\lambda_i}, \hat\tau_{\theta_j})\}_{i=1,j=0}^{N_\lambda,N_\theta}$, and $\{(\tau_{\lambda_i}, \tau_{\theta_j})\}_{i=1,j=1}^{N_\lambda,N_\theta}$, respectively, and satisfying periodic conditions in the longitudinal dimension, and the latitudinal boundary conditions

$$\begin{aligned} &U_\Delta^{n+1}(\hat\tau_{\lambda_i}, \pm\tfrac{\pi}{2}) = 0, && V_\Delta^{n+1}(\tau_{\lambda_i}, \pm\tfrac{\pi}{2}) = 0,\\ &D_\theta\phi_\Delta^{n+1}(\tau_{\lambda_i}, \pm\tfrac{\pi}{2}) = \gamma_\phi^{n+1}(\tau_{\lambda_i}, \pm\tfrac{\pi}{2}), && D_\theta\zeta_\Delta^{n+1}(\tau_{\lambda_i}, \pm\tfrac{\pi}{2}) = \gamma_\zeta^{n+1}(\tau_{\lambda_i}, \pm\tfrac{\pi}{2}), \end{aligned} \qquad (65)$$

for $i = 1, \ldots, N_\lambda$. The system (62)–(64) is solved by first eliminating the divergence terms from (64) using (62) and (63), and then linearizing and solving the resulting nonlinear Helmholtz equation using fixed-point iteration.

3 Numerical Results

In this section, we present convergence results for the OQSC methods using modified SWEs with forcing terms constructed such that an analytical solution is known a priori. The modified SWEs are described in [11]. We solved the system using the standard QSC method (52)–(55), the one-step OQSC method (45)–(51), and the two-step OQSC method (52)–(55) and (62)–(65) with grid sizes 32×32, 64×64, 128×128, and 256×256. The Arakawa C-grid was used in the spatial discretization. We used timesteps of 60 seconds (i.e., $\Delta t = 60$ s). The solution for ϕ was computed at $T = 16\frac{2}{3}$ hours and compared to the reference solution. The convergence results are shown in Table 1, where $N = N_\lambda = N_\theta$ is the number of subintervals in one dimension. Two error norms are computed for the OQSC methods: the local error norms at gridpoints and the global error norms, labelled "$|e|$" and "$||e||$," respectively, in Table 1. Only the local error norms at gridpoints are shown for the standard QSC method, which is not expected to exhibit superconvergence at special points (i.e., the local and global errors for the standard QSC method are of the same order). The error norms are computed as the ratios of the 2-norm of the difference between the numerical solution and the reference solution, to the 2-norm of the reference solution. The errors reflect the local truncation error of each method, which, in our experiments, is found to be roughly second order for standard QSC, and roughly fourth order for OQSC locally and third order globally. We estimate the convergence order of the errors by $p = -\log\left(\frac{e_1}{e_2}\right) / \log\left(\frac{N_1}{N_2}\right)$, where e_1 and e_2 are error norms corresponding to grid sizes N_1 and N_2, respectively. The computed values for p are listed in the columns labelled "p" in Table 1.

Table 1: Observed errors and respective orders of convergence for the one-step OQSC, two-step OQSC, and standard QSC methods with various spatial grid sizes.

	one-step OQSC				two-step OQSC				standard QSC	
N	$\lvert e\rvert$	p	$\lVert e\rVert$	p	$\lvert e\rvert$	p	$\lVert e\rVert$	p	$\lvert e\rvert$	p
32	1.327e-1	—	1.566e-1	—	1.524e-1	—	1.688e-1	—	2.105e-1	—
64	9.267e-3	3.84	2.328e-2	2.75	9.929e-3	3.94	2.139e-2	2.98	6.215e-2	1.76
128	8.078e-4	3.52	3.274e-3	2.83	7.535e-4	3.72	2.967e-3	2.85	1.677e-2	1.89
256	6.525e-5	3.63	4.969e-4	2.72	5.410e-5	3.80	4.087e-4	2.86	4.340e-3	1.95

We measured the number of floating-point operations (flops) using MATLAB for

Table 2: Observed computational costs for the one-step OQSC, two-step OQSC and standard QSC methods with various spatial grid sizes.

	one-step OQSC		two-step OQSC		standard QSC	
N	flops	k	flops	k	flops	k
32	3.719e11	—	3.234e11	—	1.988e11	—
64	1.418e12	1.93	1.250e12	1.95	7.627e11	1.94
128	5.402e12	1.93	4.821e12	1.95	2.913e11	1.93
256	2.049e13	1.92	1.842e13	1.93	1.107e13	1.93

Table 3: Observed computational costs for the QSG and LSG methods with various spatial grid sizes.

	QSG		LSG	
N	flops	k	flops	k
32	3.952e11	—	4.947e10	—
64	1.506e12	1.93	1.892e11	1.94
128	5.745e12	1.93	7.263e11	1.94
256	2.171e13	1.92	2.765e12	1.93

the five spatial discretization methods: linear spline Galerkin (LSG), QSG, standard QSC, and one-step and two-step OQSC methods; the results are shown in Tables 2 and 3. (The application of the QSG method to the SWEs is described in [11]; the convergence results of LSG and QSG can also be found in [11].) We estimate the order with which the number of flops increases by $k = -\log\left(\frac{f_1}{f_2}\right)/\log\left(\frac{N_1}{N_2}\right)$, where f_1 and f_2 are the number of flops corresponding to grid sizes N_1 and N_2, respectively. The computed values for k are listed in the columns labelled "k" in Tables 2 and 3. At each fixed-point iteration, the conjugate gradient (CG) iterative method was used to solve the linearized Helmholtz equation (see appendix of [11] for details), and the matrices are stored in sparse format. Thus, the computational cost per CG iteration should increase by a factor of four when N, the number of subintervals in one dimension, is doubled. Therefore, if the number of CG iterations were to stay about the same as N increases, the total work in the method should increase by about a factor of four. In these experiments, however, the flop counts showed sub-quadratic increase, as slightly fewer CG iterations were required as N increased. In our experiments, we noticed a small decrease in the condition number of the matrix associated with the linear Helmholtz equation when the grid size increases, and this possibly explains the small decrease in the number of CG iterations. The QSG method is more expensive than the OQSC methods because the former involves computing inner products using quadrature rules [11], an expense not required by the collocation methods.

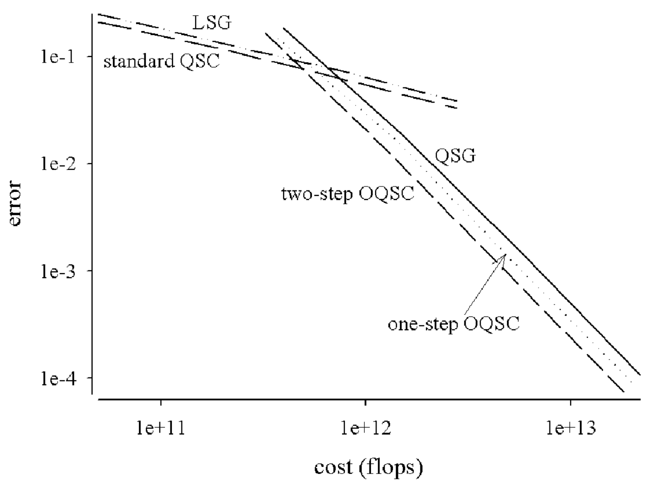

Figure 1: A log-log scale plot of the errors versus computational costs, measured as the total number of flops, for different methods.

Figure 1 compares the efficiency of the methods. Although the high-order methods (i.e., OQSC and QSG) require more computational work than the low-order methods (i.e., QSC and LSG) for a given grid size, the former are more efficient for large systems ($N > 50$ in this problem). This is because the cost for all methods considered increases at about the same rate, but the accuracy for the high-order methods increases much more rapidly than for the low-order methods. Among the high-order methods, the two-step OQSC method is the most efficient for our problem.

4 Comparison of Staggering Schemes

In this section, we incorporate three staggering schemes, namely the Arakawa A-grid, B-grid, and C-grid, which are depicted in Figure 2, into our discretization methods, and analyze their performance. We concentrate on the group velocities of gravity waves, the accuracy of which is sensitive to the choice of discretization scheme. Our analysis is carried out on the simplified SWEs

$$\frac{du}{dt} - f^*v + \frac{\phi_\lambda}{R\cos\Theta^*} = 0, \tag{66}$$

$$\frac{dv}{dt} + f^*u + \frac{\phi_\theta}{R} = 0, \tag{67}$$

$$\frac{d\phi}{dt} + \frac{\Phi^*}{R}\left(\frac{u_\lambda}{\cos\Theta^*} + v_\theta\right) = 0, \tag{68}$$

with biperiodic boundary conditions, constant f^*, Φ^* and Θ^*, and constant coefficients u^* and v^* in the Lagrangian derivative $d/dt = \partial/\partial t + u^*/(R\cos\Theta^*)\ \partial/\partial\lambda + v^*/R\ \partial/\partial\theta$. For each of the A-, B- and C-grids, and each of the numerical methods considered, we derive formulae for the wave frequencies and the respective group velocities. To study the sign of the numerical group velocities, which indicates whether energy propagates in the proper direction, we compute and plot them assuming a normalized system with $\Phi^* = 1$, $R = 1$, $\Theta^* = 0$ and $f^* = 0$, with the additional assumption that the mean wind speeds are zero, i.e. $u^* = v^* = 0$, and with $\Delta t = 0.1$, $\Delta\lambda = 0.25$ and $\Delta\theta = 0.25$.

The analysis shows that care must be taken in choosing an appropriate discretization scheme, otherwise energy associated with short gravity waves may propagate in the wrong direction. This conclusion is consistent with the general agreement in the literature [3, 8] and is also supported by numerical experiments involving equatorial Kelvin waves.

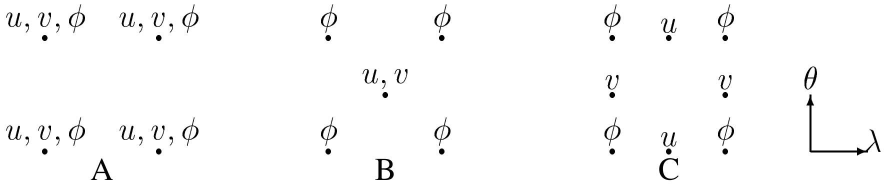

Figure 2: A schematic diagram of the Arakawa A-, B-, and C-grids.

4.1 The Continuous Case

We first examine the continuous problem. Assume that the solution to (66)–(68) is of the form

$$\begin{pmatrix} u(\lambda,\theta,t) \\ v(\lambda,\theta,t) \\ \phi(\lambda,\theta,t) \end{pmatrix} = \begin{pmatrix} u_0 \\ v_0 \\ \phi_0 \end{pmatrix} e^{\imath(k\lambda + l\theta + \omega t)}, \tag{69}$$

where k and l are the longitudinal and latitudinal wave numbers, respectively, ω denotes the wave frequency and $\nu \equiv \frac{u^*}{R\cos\Theta^*} + \frac{v^*}{R} + \omega$ denotes the Lagrangian frequency.

To compute the Lagrangian frequency of the true solution, (69) is substituted into (66)–(68), resulting in a 3×3 system of equations for u_0, v_0, and ϕ_0. Then, by setting the determinant of the system to zero, an expression for ν can be obtained. This expression can then be solved to yield the gravity wave frequencies

$$\begin{aligned} \omega^{\pm} &= \nu - \frac{u^*}{R\cos\Theta^*} - \frac{v^*}{R} \\ &= -\frac{u^*}{R\cos\Theta^*} - \frac{v^*}{R} \pm \sqrt{\Phi^* \left[\left(\frac{k}{R\cos\Theta^*} \right)^2 + \left(\frac{l}{R} \right)^2 \right] + f^{*2}}. \end{aligned} \tag{70}$$

The group velocities of the gravity waves in the λ-dimension are given by

$$c_\lambda^{\pm} \equiv \frac{d\omega^{\pm}}{dk} = \pm \frac{\Phi^* \frac{k}{(R\cos\Theta^*)^2}}{\sqrt{\Phi^* \left[\left(\frac{k}{R\cos\Theta^*} \right)^2 + \left(\frac{l}{R} \right)^2 \right] + f^{*2}}}, \tag{71}$$

while in the θ-dimension the group velocities are given by

$$c_\theta^{\pm} \equiv \frac{d\omega^{\pm}}{dl} = \pm \frac{\Phi^* \frac{l}{R^2}}{\sqrt{\Phi^* \left[\left(\frac{k}{R\cos\Theta^*} \right)^2 + \left(\frac{l}{R} \right)^2 \right] + f^{*2}}}. \tag{72}$$

We will focus on the positive components of the group velocities in the λ-dimension, i.e., c_λ^+. The group velocities for the continuous solution in the λ-dimension are plotted versus the wave numbers in Figures 3. Note that $c_\lambda^+ \geq 0$ for all wavelengths. Similarly, it can be shown that $c_\theta^+ \geq 0$ for all wavelengths [13].

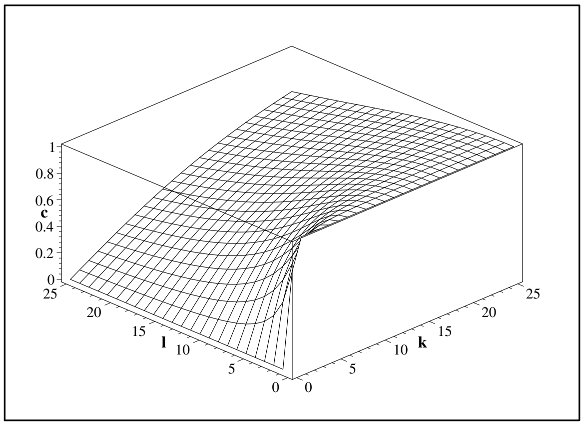

Figure 3: Group velocities of continuous gravity solution in the λ-direction. All waves travel with positive velocities.

4.2 The A-grid

We study the case of the unstaggered grid with each of the proposed methods. Let p_k, p_{λ_k}, q_l, and q_{θ_l} be the eigenvalues associated with the longitudinal mass matrix P, the longitudinal first-derivative matrix P_λ, the latitudinal mass matrix Q, and the latitudinal first-derivative matrix Q_θ, respectively. These matrices and the respective eigenvalues are different for each of the QSG, QSC, and OQSC methods. The matrices are shown explicitly in the appendix of [13]. The expressions for p_k and p_{λ_k} for the QSG, QSC, and OQSC methods are given in Table 4; the derivations can be found in the appendix of [13]. The expressions for q_l and q_{θ_l} are similar.

It is easy to see that, due to periodicity, P and P_λ are circulant and thus they share the same eigenvector $\vartheta_k = \left(e^{\imath kj\Delta\lambda}\right)_{j=0}^{N_\lambda-1}$. Similarly, Q and Q_θ share the same eigenvector $\vartheta_l' = \left(e^{\imath lj\Delta\theta}\right)_{j=0}^{N_\theta-1}$. For convenience, in the following we omit the subscripts k and l from the eigenvalues.

It turns out that the study of the QSG, QSC and one-step OQSC methods is similar, while that of two-step OQSC is different.

Table 4: Eigenvalues of unstaggered discrete operators in the λ-dimension

QSG	p_k	$\frac{1}{15}\left[15 - 15\sin^2\left(\frac{k\Delta\lambda}{2}\right) + 2\sin^4\left(\frac{k\Delta\lambda}{2}\right)\right]$
	p_{λ_k}	$\imath\frac{2}{3\Delta\lambda}\sin\left(\frac{k\Delta\lambda}{2}\right)\cos\left(\frac{k\Delta\lambda}{2}\right)\left[3 - \sin^2\left(\frac{k\Delta\lambda}{2}\right)\right]$
	$p_{\lambda\lambda_k}$	$\frac{4}{3\Delta\lambda^2}\sin^2\left(\frac{k\Delta\lambda}{2}\right)\left[-3 + 2\sin^2\left(\frac{k\Delta\lambda}{2}\right)\right]$
QSC, two-step OQSC	p_k	$1 - \frac{1}{2}\sin^2\left(\frac{k\Delta\lambda}{2}\right)$
	p_{λ_k}	$\imath\frac{2}{\Delta\lambda}\sin\left(\frac{k\Delta\lambda}{2}\right)\cos\left(\frac{k\Delta\lambda}{2}\right)$
	$p_{\lambda\lambda_k}$	$-\frac{4}{\Delta\lambda^2}\sin^2\left(\frac{k\Delta\lambda}{2}\right)$
one-step OQSC	p_k	$1 - \frac{1}{2}\sin^2\left(\frac{k\Delta\lambda}{2}\right)$
	p_{λ_k}	$\imath\frac{2}{\Delta\lambda}\sin\left(\frac{k\Delta\lambda}{2}\right)\cos\left(\frac{k\Delta\lambda}{2}\right)\left[1 + \frac{1}{6}\sin^2\left(\frac{k\Delta\lambda}{2}\right)\right]$
	$p_{\lambda\lambda_k}$	$\imath\frac{1}{6\Delta\lambda}\sin\left(\frac{k\Delta\lambda}{2}\right)\left[9 + 2\cos\left(\frac{k\Delta\lambda}{2}\right)\right]$

4.2.1 QSG, QSC, and One-Step OQSC Methods

The Lagrangian frequencies of the discrete solution computed with the QSG, the standard QSC, and the one-step OQSC methods on the A-grid have been shown in [11] to be

$$\nu = \frac{1}{\Delta t}\arctan\left(\frac{\pm 4\sqrt{AB}}{4A - B}\right), \tag{73}$$

where $A = (R\cos\Theta^* pq)^2$ and $B = (\Delta t f^* R\cos\Theta^* pq)^2 - \Delta t^2\Phi^*(p_\lambda^2 q^2 + \cos^2\Theta^* p^2 q_\theta^2)$, and where p, q, p_λ, and q_θ are different for each method. Then, using (70), we can compute the wave frequencies of the numerical solution by

$$\omega^{\pm} = -\frac{u^*}{R\cos\Theta^*} - \frac{v^*}{R} + \frac{1}{\Delta t}\arctan\left(\frac{\pm 4\sqrt{AB}}{4A - B}\right). \tag{74}$$

Note that both A and B vary with k or l, since they are functions of the eigenvalues p, p_λ, q, and q_θ, which in turn depend on the wave numbers k and l.

From (74) we derive formulae for the group velocities $\frac{d\omega^\pm}{dk}$ and $\frac{d\omega^\pm}{dl}$. In Figure 4, we plot $\frac{d\omega^+}{dk}$ corresponding to the QSC method versus the wave numbers k, for the case $\Phi^* = 1$, $R = 1$, $\Theta^* = 0$, $f^* = 0$, $u^* = v^* = 0$, $\Delta t = 0.1$, $\Delta\lambda = 0.25$, and $\Delta\theta = 0.25$. Note that the group velocities of short waves (large wave numbers) are negative, even though, according to our analysis of the continuous solutions, all gravity waves should travel in the positive direction. Similar results have been obtained for the QSG and one-step OQSC methods, and for $\frac{d\omega^+}{dl}$ [13]. Therefore, we conclude that the (unstaggered) A-grid is inaccurate in capturing the group velocities of short gravity waves.

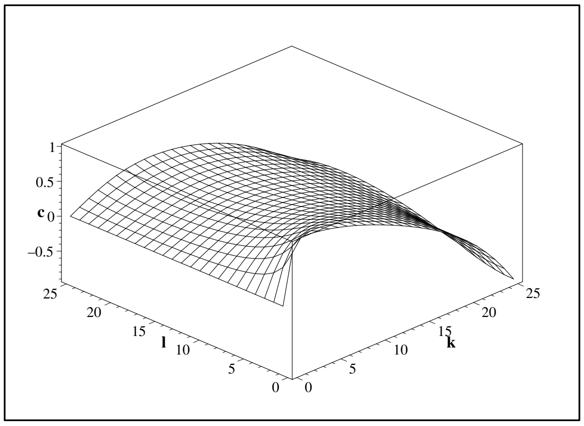

Figure 4: Group velocities of gravity waves in the λ-direction for the QSC method on an A-grid. Some waves travel with negative velocities.

4.2.2 *Two-Step OQSC Method*

In the two-step OQSC method, a second-order intermediate solution is computed first, and is then used to perturb the equations appropriately. The perturbed equations are then solved to yield a locally fourth-order solution, as described in Section 2.3. The mass and first derivative matrices for the two-step OQSC method are the same as those for the QSC method. In fact, the solution obtained from the first step of the two-step method, when the unperturbed equations are solved, *is* that of the QSC method. We denote this intermediate solution by

$$\begin{pmatrix} \breve{u}_\Delta^{n+1} \\ \breve{v}_\Delta^{n+1} \\ \breve{\phi}_\Delta^{n+1} \end{pmatrix} = \begin{pmatrix} u_0 \\ v_0 \\ \phi_0 \end{pmatrix} e^{\imath(k\lambda + l\theta + \breve{\omega}(n+1)\Delta t)}. \tag{75}$$

The Lagrangian frequency $\breve{\nu}$ of the intermediate solution is given by (73), with the eigenvalues p, q, p_λ, and q_θ given in Table 4. In the second step, because of the perturbation terms, the associated 3×3 system for u_0, v_0, and ϕ_0 is different from that derived in the previous subsection. We assume that the solution of the second step satisfies (69). Note that the Lagrangian frequency $\breve{\nu}$ of the intermediate solution may be different from the Lagrangian frequency ν of the solution of the second step. Since the equations solved in the second step of the two-step collocation method are perturbed, the eigenvalue analysis for this method needs to be done differently. For convenience, in this section, we denote by L_λ and L_θ the matrices arising from the one-dimensional difference operators Λ'_λ and Λ'_θ, respectively, with periodic boundary conditions. That is, L_λ is the almost tridiagonal $N_\lambda \times N_\lambda$ matrix with $(L_\lambda)_{i,i-1} = (L_\lambda)_{i,i+1} = 1/\Delta\lambda^2$, $(L_\lambda)_{i,i} = -2/\Delta\lambda^2$ and $(L_\lambda)_{1,N_\lambda} = (L_\lambda)_{N_\lambda,1} = 1/\Delta\lambda^2$. The matrix L_θ is defined similarly, again assuming periodic boundary conditions. Note that, for the two-step OQSC method, L_λ and L_θ are the same as the stiffness matrices $P_{\lambda\lambda}$ and $Q_{\theta\theta}$, respectively, and thus they have the same eigenvalues $p_{\lambda\lambda}$ and $q_{\theta\theta}$, respectively, which can be found in Table 4.

Following procedures similar to those outlined in [11], we obtain the following discretized perturbed equations for the A-grid:

$$\begin{aligned}
(P\otimes Q)\left(\frac{\boldsymbol{u}_\Delta^{n+1}-\tilde{\boldsymbol{u}}_\Delta^{n}}{\Delta t}\right) - f^*(P\otimes Q)\left(\frac{\boldsymbol{v}_\Delta^{n+1}+\tilde{\boldsymbol{v}}_\Delta^{n}}{2}\right) + \frac{1}{R\cos\Theta^*}(P_\lambda\otimes Q)\left(\frac{\boldsymbol{\phi}_\Delta^{n+1}+\tilde{\boldsymbol{\phi}}_\Delta^{n}}{2}\right)& \\
= -\frac{1}{R\cos\Theta^*}\frac{\Delta\lambda^2}{24}(L_\lambda\otimes I)(P_\lambda\otimes Q)\left(\frac{\breve{\boldsymbol{\phi}}_\Delta^{n+1}+\tilde{\boldsymbol{\phi}}_\Delta^{n}}{2}\right)&, \quad (76)
\end{aligned}$$

$$\begin{aligned}
(P\otimes Q)\left(\frac{\boldsymbol{v}_\Delta^{n+1}-\tilde{\boldsymbol{v}}_\Delta^{n}}{\Delta t}\right) + f^*(P\otimes Q)\left(\frac{\boldsymbol{u}_\Delta^{n+1}+\tilde{\boldsymbol{u}}_\Delta^{n}}{2}\right) + \frac{1}{R}(P\otimes Q_\theta)\left(\frac{\boldsymbol{\phi}_\Delta^{n+1}+\tilde{\boldsymbol{\phi}}_\Delta^{n}}{2}\right)& \\
= -\frac{1}{R}\frac{\Delta\theta^2}{24}(I\otimes L_\theta)(P\otimes Q_\theta)\left(\frac{\breve{\boldsymbol{\phi}}_\Delta^{n+1}+\tilde{\boldsymbol{\phi}}_\Delta^{n}}{2}\right)&, \quad (77)
\end{aligned}$$

$$\begin{aligned}
(P\otimes Q)\left(\frac{\boldsymbol{\phi}_\Delta^{n+1}-\tilde{\boldsymbol{\phi}}_\Delta^{n}}{\Delta t}\right) + \frac{\Phi^*}{R\cos\Theta^*}(P_\lambda\otimes Q)\left(\frac{\boldsymbol{u}_\Delta^{n+1}+\tilde{\boldsymbol{u}}_\Delta^{n}}{2}\right) + \frac{\Phi^*}{R}(P\otimes Q_\theta)\left(\frac{\boldsymbol{v}_\Delta^{n+1}+\tilde{\boldsymbol{v}}_\Delta^{n}}{2}\right)& \\
= -\frac{\Phi^*}{R\cos\Theta^*}\frac{\Delta\lambda^2}{24}(L_\lambda\otimes I)(P_\lambda\otimes Q)\left(\frac{\breve{\boldsymbol{u}}_\Delta^{n+1}+\tilde{\boldsymbol{u}}_\Delta^{n}}{2}\right)& \\
-\frac{\Phi^*}{R}\frac{\Delta\theta^2}{24}(I\otimes L_\theta)(P\otimes Q_\theta)\left(\frac{\breve{\boldsymbol{v}}_\Delta^{n+1}+\tilde{\boldsymbol{v}}_\Delta^{n}}{2}\right)&. \quad (78)
\end{aligned}$$

The boldface type is used to denote vectors of function values at collocation points. Rewriting equations (76)–(78) in terms of the eigenvalues and simplifying, we obtain

$$\begin{aligned}
&pq\left(\frac{e^{\imath\nu\Delta t}-1}{\Delta t}\right)u_0 - f^*pq\left(\frac{e^{\imath\nu\Delta t}+1}{2}\right)v_0 + \frac{p_\lambda q}{R\cos\Theta^*}\left(\frac{e^{\imath\nu\Delta t}+1}{2}\right)\phi_0 \\
&\quad = -\frac{1}{R\cos\Theta^*}\frac{\Delta\lambda^2}{24}p_{\lambda\lambda}p_\lambda q\left(\frac{e^{\imath\breve{\nu}\Delta t}+1}{2}\right)\phi_0, \quad (79)
\end{aligned}$$

$$pq\left(\frac{e^{\imath\nu\Delta t}-1}{\Delta t}\right)v_0 + f^* pq\left(\frac{e^{\imath\nu\Delta t}+1}{2}\right)u_0 + \frac{pq_\theta}{R}\left(\frac{e^{\imath\nu\Delta t}+1}{2}\right)\phi_0$$
$$= -\frac{1}{R}\frac{\Delta\theta^2}{24}pq_{\theta\theta}q_\theta\left(\frac{e^{\imath\breve{\nu}\Delta t}+1}{2}\right)\phi_0, \tag{80}$$
$$pq\left(\frac{e^{\imath\nu\Delta t}-1}{\Delta t}\right)\phi_0 + \frac{\Phi^*}{R\cos\Theta^*}p_\lambda q\left(\frac{e^{\imath\nu\Delta t}+1}{2}\right)u_0 + \frac{\Phi^*}{R}pq_\theta\left(\frac{e^{\imath\nu\Delta t}+1}{2}\right)v_0$$
$$= -\frac{\Phi^*}{R\cos\Theta^*}\frac{\Delta\lambda^2}{24}p_{\lambda\lambda}p_\lambda q\left(\frac{e^{\imath\breve{\nu}\Delta t}+1}{2}\right)u_0 - \frac{\Phi^*}{R}\frac{\Delta\theta^2}{24}pq_{\theta\theta}q_\theta\left(\frac{e^{\imath\breve{\nu}\Delta t}+1}{2}\right)v_0. \tag{81}$$

By setting the determinant of the above system to zero, and solving for $e^{\imath\nu\Delta t}$, we find that

$$\omega^\pm = -\frac{u^*}{R\cos\Theta^*} - \frac{v^*}{R} + \frac{1}{\Delta t}\text{arctan}\left[\frac{\mathcal{I}m(\mathcal{F}_A^\pm)}{\mathcal{R}e(\mathcal{F}_A^\pm)}\right], \tag{82}$$

where

$$\mathcal{F}_A^\pm \equiv \frac{4A - B + C \pm 2\imath\sqrt{4A(B-C) + (4+f^{*2})(\delta\lambda^2 + \cos\Theta^{*2}\delta\theta^2)A + D}}{4A+B}, \tag{83}$$

and

$$A = (R\cos\Theta^* pq)^2,$$
$$B = (\Delta t f^* R\cos\Theta^* pq)^2 - \Delta t^2\Phi^*(p_\lambda^2 q^2 + \cos^2\Theta^* p^2 q_\theta^2),$$
$$C = 2\Delta t^2\Phi^*(p_\lambda q\delta\lambda + \cos^2\Theta^* pq_\theta\delta\theta),$$
$$D = \Delta t^4\Phi^{*2}\cos^2\Theta^*(pq_\theta\delta\lambda - p_\lambda q\delta\theta)^2,$$
$$\delta\lambda = \frac{\Delta\lambda^2}{24}p_{\lambda\lambda}p_\lambda q\left(\frac{e^{\imath\breve{\nu}\Delta t}+1}{2}\right),$$
$$\delta\theta = \frac{\Delta\theta^2}{24}pq_{\theta\theta}q_\theta\left(\frac{e^{\imath\breve{\nu}\Delta t}+1}{2}\right).$$

From (82) we derive formulae for the group velocities $\frac{d\omega^\pm}{dk}$ and $\frac{d\omega^\pm}{dl}$, corresponding to the two-step OQSC method on the A-grid. We verified that, for the case $\Phi^* = 1$, $R = 1$, $\Theta^* = 0$, $f^* = 0$, $u^* = v^* = 0$, $\Delta t = 0.1$, $\Delta\lambda = 0.25$, and $\Delta\theta = 0.25$, $\frac{d\omega^+}{dk}$ for large k and $\frac{d\omega^+}{dl}$ for large l are negative. Thus the (unstaggered) A-grid does not accurately capture the group velocities of short gravity waves.

4.3 The B-grid

On the B-grid, the wind speed components u and v are computed at the same locations, while the geopotential ϕ is evaluated at points that are staggered with respect to the u, v-grid in both the λ- and θ-directions. Let $P^{\Delta \to \hat{\Delta}}$ and $P^{\hat{\Delta} \to \Delta}$ be the longitudinal staggered mass matrices, and $P_\lambda^{\Delta \to \hat{\Delta}}$ and $P_\lambda^{\hat{\Delta} \to \Delta}$ be the respective first-derivative matrices. Recall that these matrices are different for each of the QSG, QSC and OQSC methods, and are shown explicitly in the appendix of [13].

Recall that $\vartheta_k = \left(e^{\imath kj\Delta\lambda}\right)_{j=0}^{N_\lambda - 1}$. Let $\hat{\vartheta}_k = \left(e^{\imath k(j+\frac{1}{2})\Delta\lambda}\right)_{j=0}^{N_\lambda - 1}$ for $k = 0, \ldots, N_\lambda - 1$, and observe that the staggering operators satisfy the following conditions:

$$
\begin{aligned}
P^{\Delta \to \hat{\Delta}} \vartheta_k &= p_k^{\to} \hat{\vartheta}_k, \qquad & P^{\hat{\Delta} \to \Delta} \hat{\vartheta}_k &= p_k^{\to} \vartheta_k, \\
P_\lambda^{\Delta \to \hat{\Delta}} \vartheta_k &= p_{\lambda_k}^{\to} \hat{\vartheta}_k \qquad & P_\lambda^{\hat{\Delta} \to \Delta} \hat{\vartheta}_k &= p_{\lambda_k}^{\to} \vartheta_k.
\end{aligned}
$$

Since $\hat{\vartheta}_k = e^{\imath \frac{k}{2}\Delta\lambda} \vartheta_k$, we see that ϑ_k is an eigenvector of $P^{\Delta \to \hat{\Delta}}$ and $P_\lambda^{\Delta \to \hat{\Delta}}$, with $p_k^{\to} e^{\imath \frac{k}{2}\Delta\lambda}$ and $p_{\lambda_k}^{\to} e^{\imath \frac{k}{2}\Delta\lambda}$ being the associated eigenvalues, respectively. Similarly, $\hat{\vartheta}_k$ is an eigenvector of $P^{\hat{\Delta} \to \Delta}$ and $P_\lambda^{\hat{\Delta} \to \Delta}$, with $p_k^{\to} e^{-\imath \frac{k}{2}\Delta\lambda}$ and $p_{\lambda_k}^{\to} e^{-\imath \frac{k}{2}\Delta\lambda}$ being the associated eigenvalues, respectively. The arrows in $p_k^{\to}$ and $p_{\lambda_k}^{\to}$ indicate that these scalars are associated with staggering operators. The scalars $p_k^{\to}$ and $p_{\lambda_k}^{\to}$ take on different values depending on the spatial discretization method (see Table 5; the derivations can be found in [13]). Similar relations hold for the corresponding staggering operators in the θ-direction.

Table 5: Scaled eigenvalues of staggering discrete operators in the λ-dimension

QSG	$p_k^{\to}$	$\frac{1}{120}\cos\left(\frac{k\Delta\lambda}{2}\right)\left[120 - 60\sin^2\left(\frac{k\Delta\lambda}{2}\right) + \sin^4\left(\frac{k\Delta\lambda}{2}\right)\right]$
	$p_{\lambda_k}^{\to}$	$\imath\frac{32}{\Delta\lambda}\sin\left(\frac{k\Delta\lambda}{2}\right)\left[24 - 20\sin^2\left(\frac{k\Delta\lambda}{2}\right) + \sin^4\left(\frac{k\Delta\lambda}{2}\right)\right]$
QSC, two-step	$p_k^{\to}$	$\cos\left(\frac{k\Delta\lambda}{2}\right)$
	$p_{\lambda_k}^{\to}$	$\imath\frac{2}{\Delta\lambda}\sin\left(\frac{k\Delta\lambda}{2}\right)$
OQSC one-step	p_{λ_k}	$\imath\frac{2}{\Delta\lambda}\sin\left(\frac{k\Delta\lambda}{2}\right)\cos\left(\frac{k\Delta\lambda}{2}\right)\left[1 + \frac{1}{6}\sin^2\left(\frac{k\Delta\lambda}{2}\right)\right]$
OQSC	$p_{\lambda_k}^{\to}$	$\imath\frac{1}{6\Delta\lambda}\sin\left(\frac{k\Delta\lambda}{2}\right)\left[9 + 2\cos\left(\frac{k\Delta\lambda}{2}\right)\right]$

4.3.1 QSG, QSC, and One-Step OQSC Methods

Following the procedures described in [11], we discretize (66)–(68) in time, rewrite the resulting equations in terms of the eigenvalues, and obtain the following equations after some simplifications:

$$pq\left(\frac{e^{\imath\nu\Delta t}-1}{\Delta t}\right)u_0 - f^*pq\left(\frac{e^{\imath\nu\Delta t}+1}{2}\right)v_0 + \frac{p_\lambda^{\rightarrow}q^{\rightarrow}}{R\cos\Theta^*}\left(\frac{e^{\imath\nu\Delta t}+1}{2}\right)\phi_0 = 0, \tag{84}$$

$$pq\left(\frac{e^{\imath\nu\Delta t}-1}{\Delta t}\right)v_0 + f^*pq\left(\frac{e^{\imath\nu\Delta t}+1}{2}\right)u_0 + \frac{p^{\rightarrow}q_\theta^{\rightarrow}}{R}\left(\frac{e^{\imath\nu\Delta t}+1}{2}\right)\phi_0 = 0, \tag{85}$$

$$pq\left(\frac{e^{\imath\nu\Delta t}-1}{\Delta t}\right)\phi_0 + \frac{\Phi^*}{R\cos\Theta^*}p_\lambda^{\rightarrow}q^{\rightarrow}\left(\frac{e^{\imath\nu\Delta t}+1}{2}\right)u_0 + \frac{\Phi^*}{R}p^{\rightarrow}q_\theta^{\rightarrow}\left(\frac{e^{\imath\nu\Delta t}+1}{2}\right)v_0 = 0. \tag{86}$$

The solution for the Lagrangian frequency for the B-grid is given by the relations

$$e^{\imath\nu\Delta t} = 1, \quad \frac{4A - B \pm 4\imath\sqrt{AB}}{4A+B}, \tag{87}$$

where $A = (R\cos\Theta^* pq)^2$ and $B = (\Delta t f^* R\cos\Theta^* pq)^2 - \Delta t^2\Phi^*({p_\lambda^{\rightarrow}}^2 {q^{\rightarrow}}^2 + \cos^2\Theta^* {p^{\rightarrow}}^2 {q_\theta^{\rightarrow}}^2)$.

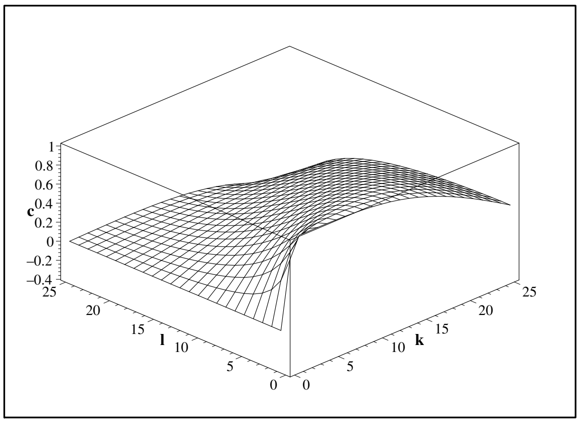

Figure 5: Group velocities of gravity waves in the λ-direction for the QSC method on a B-grid. Some short waves propagate with negative velocities.

From (87), we can derive the Lagrangian frequency ν and the wave frequency $\omega^{\pm}$ on a B-grid. In Figure 5, we plot $\frac{d\omega^+}{dk}$ corresponding to the QSC method versus the wave numbers k, for the case $\Phi^* = 1$, $R = 1$, $\Theta^* = 0$, $f^* = 0$, $u^* = v^* = 0$,

$\Delta t = 0.1$, $\Delta\lambda = 0.25$, and $\Delta\theta = 0.25$. As with the A-grid, energy propagates in the wrong direction at small scales, although the problem is less severe in this case. Similar results have been obtained for the QSG and one-step OQSC methods, and for $\frac{d\omega^+}{dl}$ [13].

4.3.2 Two-Step OQSC Method

The analogous eigenvalue equations for the two-step OQSC method are

$$\begin{aligned}
&pq\left(\frac{e^{\imath\nu\Delta t}-1}{\Delta t}\right)u_0 - f^*pq\left(\frac{e^{\imath\nu\Delta t}+1}{2}\right)v_0 + \frac{p_\lambda^{\rightarrow}q^{\rightarrow}}{R\cos\Theta^*}\left(\frac{e^{\imath\nu\Delta t}+1}{2}\right)\phi_0 \\
&\quad = -\frac{1}{R\cos\Theta^*}\frac{\Delta\lambda^2}{24}p_{\lambda\lambda}p_\lambda^{\rightarrow}q^{\rightarrow}\left(\frac{e^{\imath\breve{\nu}\Delta t}+1}{2}\right)\phi_0, \qquad (88)\\
&pq\left(\frac{e^{\imath\nu\Delta t}-1}{\Delta t}\right)v_0 + f^*pq\left(\frac{e^{\imath\nu\Delta t}+1}{2}\right)u_0 + \frac{p^{\rightarrow}q_\theta^{\rightarrow}}{R}\left(\frac{e^{\imath\nu\Delta t}+1}{2}\right)\phi_0 \\
&\quad = -\frac{1}{R}\frac{\Delta\theta^2}{24}p^{\rightarrow}q_{\theta\theta}q_\theta^{\rightarrow}\left(\frac{e^{\imath\breve{\nu}\Delta t}+1}{2}\right)\phi_0, \qquad (89)\\
&pq\left(\frac{e^{\imath\nu\Delta t}-1}{\Delta t}\right)\phi_0 + \frac{\Phi^*}{R\cos\Theta^*}p_\lambda^{\rightarrow}q^{\rightarrow}\left(\frac{e^{\imath\nu\Delta t}+1}{2}\right)u_0 + \frac{\Phi^*}{R}p^{\rightarrow}q_\theta^{\rightarrow}\left(\frac{e^{\imath\nu\Delta t}+1}{2}\right)v_0 \\
&\quad = -\frac{\Phi^*}{R\cos\Theta^*}\frac{\Delta\lambda^2}{24}p_{\lambda\lambda}p_\lambda^{\rightarrow}q^{\rightarrow}\left(\frac{e^{\imath\breve{\nu}\Delta t}+1}{2}\right)u_0 - \frac{\Phi^*}{R}\frac{\Delta\theta^2}{24}p^{\rightarrow}q_{\theta\theta}q_\theta^{\rightarrow}\left(\frac{e^{\imath\breve{\nu}\Delta t}+1}{2}\right)v_0. \qquad (90)
\end{aligned}$$

By moving all terms to the left side, setting the determinant of the resulting system to zero, and solving for $e^{\imath\nu\Delta t}$, we find that

$$\begin{aligned}
e^{\imath\nu\Delta t} &= 1, \frac{4A - B + C \pm 2\imath\sqrt{4A(B-C) - \Delta t^2\Phi^*(4+\Delta t^2 f^{*2})(\delta\lambda^2 + \cos\Theta^{*2}\delta\theta^2)A + D}}{4A+B} \\
&\equiv \mathcal{F}_B^{\pm}, \qquad (91)
\end{aligned}$$

where

$$\begin{aligned}
A &= (R\cos\Theta^* pq)^2, \\
B &= (\Delta t f^* R\cos\Theta^* pq)^2 - \Delta t^2\Phi^*({p_\lambda^{\rightarrow}}^2{q^{\rightarrow}}^2 + \cos^2\Theta^* {p^{\rightarrow}}^2{q_\theta^{\rightarrow}}^2), \\
C &= 2\Delta t^2\Phi^*(p_\lambda^{\rightarrow}q^{\rightarrow}\delta\lambda + \cos^2\Theta^* p^{\rightarrow}q_\theta^{\rightarrow}\delta\theta), \\
D &= \Delta t^4\Phi^{*2}\cos^2\Theta^*(p^{\rightarrow}q_\theta^{\rightarrow}\delta\lambda - p_\lambda^{\rightarrow}q^{\rightarrow}\delta\theta)^2, \\
\delta\lambda &= \frac{\Delta\lambda^2}{24}p_{\lambda\lambda}p_\lambda^{\rightarrow}q^{\rightarrow}\left(\frac{e^{\imath\breve{\nu}\Delta t}+1}{2}\right),
\end{aligned}$$

$$\delta\theta = \frac{\Delta\theta^2}{24} p^{\rightarrow} q_{\theta\theta} q_\theta^{\rightarrow} \left(\frac{e^{\imath\check{\nu}\Delta t} + 1}{2} \right).$$

We verified by graphing $|\mathcal{F}_B^{\pm}|$ using MAPLE that $|\mathcal{F}_B^{\pm}|$ is bounded by 1, so the gravity solution is bounded. The group velocities can be computed from the wave frequencies, which are given by

$$\omega^{\pm} = -\frac{u^*}{R\cos\Theta^*} - \frac{v^*}{R} + \frac{1}{\Delta t}\arctan\left[\frac{\mathcal{I}m(\mathcal{F}_B^{\pm})}{\mathcal{R}e(\mathcal{F}_B^{\pm})}\right]. \tag{92}$$

As with the QSG, QSC and one-step OQSC methods, some short gravity waves travel in the wrong direction [13].

4.4 The C-grid

The C-grid is used in our implementation of the SWEs; its structure is shown in Figure 2. In this case, the three target functions are evaluated at different locations, with the wind speed components u and v staggered with respect to the geopotential ϕ in the λ- and θ-directions, respectively.

4.4.1 QSG, QSC, and One-Step OQSC Method

With the C-grid, the eigenvalue equations are

$$pq\left(\frac{e^{\imath\nu\Delta t} - 1}{\Delta t}\right) u_0 - f^* p^{\rightarrow} q^{\rightarrow} \left(\frac{e^{\imath\nu\Delta t} + 1}{2}\right) v_0 + \frac{p_\lambda^{\rightarrow} q}{R\cos\Theta^*}\left(\frac{e^{\imath\nu\Delta t} + 1}{2}\right)\phi_0 = 0, \tag{93}$$

$$pq\left(\frac{e^{\imath\nu\Delta t} - 1}{\Delta t}\right) v_0 + f^* p^{\rightarrow} q^{\rightarrow} \left(\frac{e^{\imath\nu\Delta t} + 1}{2}\right) u_0 + \frac{p q_\theta^{\rightarrow}}{R}\left(\frac{e^{\imath\nu\Delta t} + 1}{2}\right)\phi_0 = 0, \tag{94}$$

$$pq\left(\frac{e^{\imath\nu\Delta t} - 1}{\Delta t}\right) \phi_0 + \frac{\Phi^*}{R\cos\Theta^*} p_\lambda^{\rightarrow} q \left(\frac{e^{\imath\nu\Delta t} + 1}{2}\right) u_0 + \frac{\Phi^*}{R} p q_\theta^{\rightarrow}\left(\frac{e^{\imath\nu\Delta t} + 1}{2}\right) v_0 = 0. \tag{95}$$

The solution for the Lagrangian frequency for the C-grid is given by the relations

$$e^{\imath\nu\Delta t} = 1, \quad \frac{4A - B \pm 4\imath\sqrt{AB}}{4A + B}, \tag{96}$$

where $A = (R\cos\Theta^* pq)^2$ and $B = (\Delta t f^* R\cos\Theta^* p^{\rightarrow} q^{\rightarrow})^2 - \Delta t^2 \Phi^* (p_\lambda^{\rightarrow 2} q^2 + \cos^2\Theta^* p^2 q_\theta^{\rightarrow 2})$.

From (96), we can derive the Lagrangian frequency ν and the wave frequency $\omega^{\pm}$ on a C-grid. In Figure 6, we plot $\frac{d\omega^+}{dk}$ corresponding to the QSC method versus the

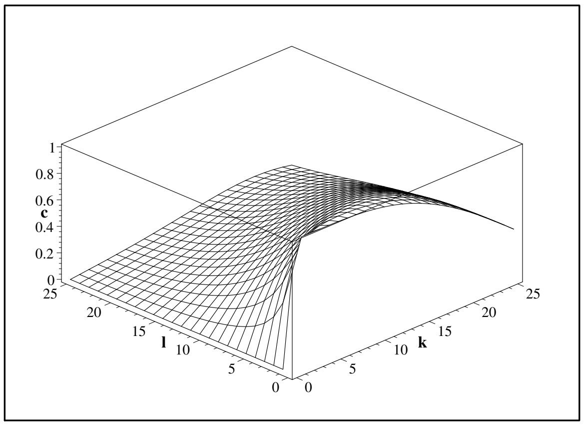

Figure 6: Group velocities of gravity waves in the λ-direction for the QSC method on a C-grid. Group velocities of all scales are positive.

wave numbers k, for the case $\Phi^* = 1$, $R = 1$, $\Theta^* = 0$, $f^* = 0$, $u^* = v^* = 0$, $\Delta t = 0.1$, $\Delta\lambda = 0.25$, and $\Delta\theta = 0.25$. In this case, the group velocities are positive for all scales, which implies that the energy propagates in the proper direction. Similar results have been obtained for the QSG and one-step OQSC methods, and for $\frac{d\omega^+}{dl}$ [13]. Hence, we conclude that the Arakawa C-grid outperforms the A- and B-grids, in that the C-grid more accurately captures the group velocities of gravity waves of all wavelengths.

4.4.2 *Two-Step OQSC Method*

For the two-step OQSC method, the eigenvalue equations are given by

$$pq\left(\frac{e^{\imath\nu\Delta t}-1}{\Delta t}\right)u_0 - f^* p^{\rightarrow} q^{\rightarrow}\left(\frac{e^{\imath\nu\Delta t}+1}{2}\right)v_0 + \frac{p_\lambda^{\rightarrow} q}{R\cos\Theta^*}\left(\frac{e^{\imath\nu\Delta t}+1}{2}\right)\phi_0$$
$$= -\frac{1}{R\cos\Theta^*}\frac{\Delta\lambda^2}{24}p_{\lambda\lambda}p_\lambda^{\rightarrow} q\left(\frac{e^{\imath\breve{\nu}\Delta t}+1}{2}\right)\phi_0, \tag{97}$$

$$pq\left(\frac{e^{\imath\nu\Delta t}-1}{\Delta t}\right)v_0 + f^* p^{\rightarrow} q^{\rightarrow}\left(\frac{e^{\imath\nu\Delta t}+1}{2}\right)u_0 + \frac{pq_\theta^{\rightarrow}}{R}\left(\frac{e^{\imath\nu\Delta t}+1}{2}\right)\phi_0$$
$$= -\frac{1}{R}\frac{\Delta\theta^2}{24}pq_{\theta\theta}q_\theta^{\rightarrow}\left(\frac{e^{\imath\breve{\nu}\Delta t}+1}{2}\right)\phi_0, \tag{98}$$

$$pq\left(\frac{e^{\imath\nu\Delta t}-1}{\Delta t}\right)\phi_0 + \frac{\Phi^*}{R\cos\Theta^*}p_\lambda^{\rightarrow} q\left(\frac{e^{\imath\nu\Delta t}+1}{2}\right)u_0 + \frac{\Phi^*}{R}pq_\theta^{\rightarrow}\left(\frac{e^{\imath\nu\Delta t}+1}{2}\right)v_0$$
$$= -\frac{\Phi^*}{R\cos\Theta^*}\frac{\Delta\lambda^2}{24}p_{\lambda\lambda}p_\lambda^{\rightarrow} q\left(\frac{e^{\imath\breve{\nu}\Delta t}+1}{2\cos\Theta^*}\right)u_0 - \frac{\Phi^*}{R}\frac{\Delta\theta^2}{24}pq_{\theta\theta}q_\theta^{\rightarrow}\left(\frac{e^{\imath\breve{\nu}\Delta t}+1}{2}\right)v_0. \tag{99}$$

By moving all terms to the left side, setting the determinant of the resulting system to zero, and solving for $e^{\imath\nu\Delta t}$, we find that

$$
\begin{aligned}
e^{\imath\nu\Delta t} = 1, \frac{4A - B + C}{4A + B} \\
&\pm \frac{2\imath\sqrt{4A(B-C) - \Delta t^2\Phi^*[4A + (\Delta t f^* R\cos\Theta^* p^{\rightarrow} q^{\rightarrow})^2](\delta\lambda^2 + \cos\Theta^{*2}\delta\theta^2) + D}}{4A + B} \\
&\equiv \mathcal{F}_C^{\pm}, \qquad (100)
\end{aligned}
$$

where

$$
\begin{aligned}
A &= (R\cos\Theta^* pq)^2, \\
B &= (\Delta t f^* R\cos\Theta^* p^{\rightarrow} q^{\rightarrow})^2 - \Delta t^2\Phi^*(p_\lambda^{\rightarrow 2} q^2 + \cos^2\Theta^* p^2 q_\theta^{\rightarrow 2}), \\
C &= 2\Delta t^2\Phi^*(p_\lambda^{\rightarrow} q\delta\lambda + \cos^2\Theta^* p q_\theta^{\rightarrow}\delta\theta), \\
D &= \Delta t^4\Phi^{*2}\cos^2\Theta^*(p q_\theta^{\rightarrow}\delta\lambda - p_\lambda^{\rightarrow} q\delta\theta)^2, \\
\delta\lambda &= \frac{\Delta\lambda^2}{24} p_{\lambda\lambda} p_\lambda^{\rightarrow} q \left(\frac{e^{\imath\breve{\nu}\Delta t} + 1}{2}\right), \\
\delta\theta &= \frac{\Delta\theta^2}{24} p q_{\theta\theta} q_\theta^{\rightarrow} \left(\frac{e^{\imath\breve{\nu}\Delta t} + 1}{2}\right).
\end{aligned}
$$

Again, we verified by graphing $|\mathcal{F}_C^{\pm}|$ using MAPLE that $|\mathcal{F}_C^{\pm}|$ is bounded by 1, so the gravity solutions are bounded. The group velocities can be computed from the wave frequencies, which are given by

$$
\omega^{\pm} = -\frac{u^*}{R\cos\Theta^*} - \frac{v^*}{R} + \frac{1}{\Delta t}\text{arctan}\left[\frac{\mathcal{I}m(\mathcal{F}_C^{\pm})}{\mathcal{R}e(\mathcal{F}_C^{\pm})}\right]. \qquad (101)
$$

As with the QSG, QSC and one-step OQSC methods, all gravity waves travel in the proper direction [13].

4.5 The Equatorial Kelvin Wave

We now demonstrate numerically the effects staggering has on group velocities of short gravitational waves. The nonlinear equatorial Kelvin wave, investigated by Boyd [1], is used as the test case in this study. Equations (50)–(52) in [11] are integrated with a new set of initial conditions:

$$
u(\lambda, \theta, 0) = \frac{1}{3} e^{-(R\theta)^2/2 - (R\lambda\cos\theta/\Delta\lambda)^2}, \qquad (102)
$$

$$v(\lambda, \theta, 0) = 0, \tag{103}$$

$$\phi'(\lambda, \theta, 0) = \frac{1}{3} e^{-(R\theta)^2/2-(R\lambda\cos\theta/\Delta\lambda)^2}. \tag{104}$$

The above initial conditions generate equatorially trapped gravity waves, traveling eastward, with wavelengths of the order of the longitudinal grid spacing. Results for the two-step OQSC method are shown in Figure 7. The simulations were run for 8 non-dimensional time units on a 64×64 grid. Similar results are also obtained using the QSG and one-step OQSC methods.

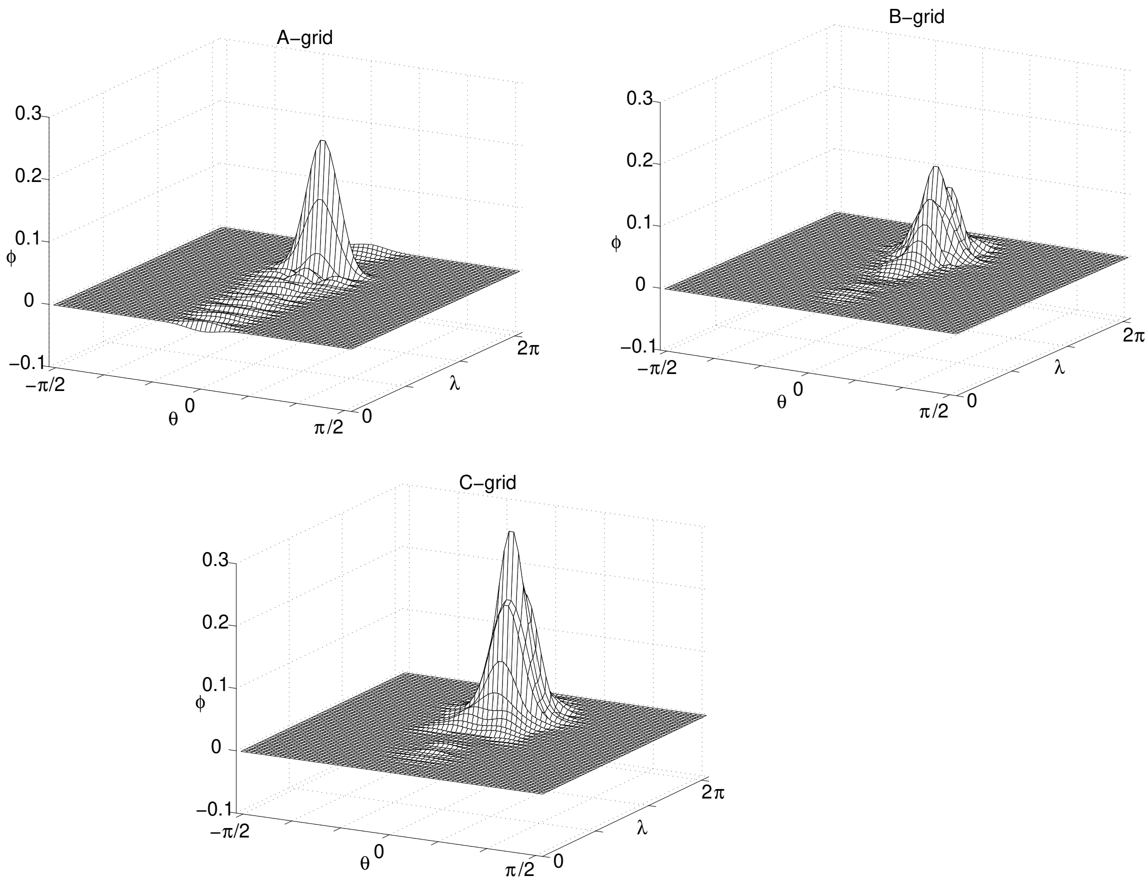

Figure 7: Simulation of gravity waves propagating eastward (in the increasing λ-direction) with the two-step OQSC method on A-, B-, and C-grids. On both the A- and B-grids, some gravity waves propagate in the wrong direction (in the decreasing λ-direction). In contrast, on the C-grid, the group velocities of waves of all wavelengths have been captured correctly.

When the A- or B-grid is used, short gravity waves are observed to propagate westward, which is the wrong direction, thus demonstrating the failure of both the A- and B-grids to faithfully capture the group velocity of short gravity waves. In contrast, gravity waves of all scales propagate in the right direction (i.e., eastward) when the C-grid is used.

5 Remarks

In this paper and in the companion paper [11], we propose high-order finite element methods for solving the SWEs on the sphere. We consider these methods a step foward in the quest for alternatives to the commonly used spectral transform methods [9, 14, 15] or low-order finite difference/finite element methods [4, 5]. In [11] we present a numerical method that combines the two-level SLSI time integration method and the QSG method; and in this paper, we combine the two-level SLSI method with the OQSC methods. Previous studies of OQSC methods are limited to unstaggered grids [2, 10]. We extend the OQSC methods to a system of three two-dimensional first-order differential equations on staggered grids.

The current implementations of the QSG and OQSC methods are done on the uniform latitude-longitude grid, in which the meridians converge at the poles. With the SLSI time discretization, numerical stability is maintained even with a Courant-Friederich-Levy (CFL) number greater than one, so there is no severe restriction on the timestep. Nevertheless, much of the computational work done at gridpoints near the poles is unnecessary. Therefore, it is a worthwhile challenge to extend the QSG and OQSC methods to skipped grids, in which the number of longitudinal gridpoints decreases toward the poles. Göttelmann solved the SWEs on a skipped grid, using a combination of the forward Euler method and the linear spline collocation method [7]. We plan to develop SLSI high-order spline-based methods for the skipped grid.

References

[1] J. P. Boyd. The nonlinear equatorial Kelvin wave. *J. of Phys. Oceanogr.*, 10:1–11, January 1980.

[2] C. C. Christara. Quadratic spline collocation methods for elliptic partial differential equations. *BIT*, 34(1):33–61, 1994.

[3] J. Côté. Variable resolution techniques for weather prediction. *Meteorol. Atmos. Phys.*, 63:31–38, 1997.

[4] J. Côté, J.-G. Desmarais, S. Gravel, A. Méthot, A. Patoine, M. Roch, and A. Staniforth. The operational CMC-MRB Global Environment Multiscale (GEM) model. Part II: Results. *Mon. Wea. Rev.*, 126:1397–1416, June 1998.

[5] J. Côté, S. Gravel, A. Méthot, A. Patoine, M. Roch, and A. Staniforth. The operational CMC-MRB Global Environmental Multiscale (GEM) model. Part I: Design considerations and formulation. *Mon. Wea. Rev.*, 126:1373–1395, June 1998.

[6] J. Côté and A. Staniforth. An accurate and efficient finite-element global model of the shallow water equations. *Mon. Wea. Rev.*, 118:2707–2717, December 1990.

[7] J. Göttelmann. A spline collocation scheme for the spherical shallow water equations. *J. Comput. Phys.*, 148(2):291–298, 1999.

[8] G. J. Haltiner and R. T. Williams. *Numerical Prediction and Dynamic Meteorology*. John Wiley and Sons, 1980.

[9] M. Hortal. Aspects of the numerics of the ECMWF model. In *Proceedings of a seminar held at ECMWF on recent developments in numerical methods for atmospheric modelings*, pages 127–143, 1999.

[10] E. N. Houstis, C. C. Christara, and J. R. Rice. Quadratic-spline collocation methods for two-point boundary value problems. *Int. J. Numer. Methods Eng.*, 26:935–952, 1988.

[11] A. T. Layton, C. C. Christara, and K. R. Jackson. Quadratic spline Galerkin method for the shallow water equation on the sphere. Submitted to *Mathematics and Computers in Simulation*, 2002.

[12] K. S. Ng. Quadratic spline collocation methods for systems of elliptic PDEs. http://www.cs.toronto.edu/pub/reports/na/ccc/ngkit-00-msc.ps.Z, M.Sc. Thesis, Department of Computer Science, University of Toronto, Toronto, Ontario, Canada, April 2000.

[13] A. W. Tam. High-order spatial discretization methods for the shallow water equations. http://www.cs.toronto.edu/pub/reports/na/tam-01-phd.ps.Z, Ph.D. Thesis, Department of Computer Science, University of Toronto, Toronto, Ontario, Canada, February 2001.

[14] D. L. Williamson and J. G. Olson. Climate simulations with a semi-Lagrangian version of the NCAR Community Climate Model. *Mon. Wea. Rev.*, 122:1594–1610, July 1994.

[15] D. L. Williamson, J. G. Olson, and B. A. Boville. A comparison of semi-Lagragnain and Eulerian tropical climate simulations. *Mon. Wea. Rev.*, 126:1001–1012, April 1998.